Parsec-scale dust distributions in Seyfert galaxies[*]

Results of the MIDI AGN snapshot survey

K. R. W. Tristram[1], D. Raban[2], K. Meisenheimer[3], W. Jaffe[2], H. Röttgering[2], L. Burtscher[3], W. D. Cotton[4], U. Graser[3], Th. Henning[3], Ch. Leinert[3], B. Lopez[5], S. Morel[6], G. Perrin[7], M. Wittkowski[8]

[1] Max-Planck-Institut für Radioastronomie, Auf dem Hügel 69, 53121 Bonn, Germany
email: tristram@mpifr-bonn.mpg.de
[2] Leiden Observatory, Leiden University, Niels-Bohr-Weg 2, 2300 CA Leiden, The Netherlands
[3] Max-Planck-Institut für Astronomie, Königstuhl 17, 69117 Heidelberg, Germany
[4] NRAO, 520 Edgemont Road, Charlottesville, VA 22903-2475, USA
[5] Laboratoire H. Fizeau, UMR 6525, Université de Nice-Sofia et Obs. de la Côte d'Azur, BP 4229, 06304 Nice Cedex 4, France.
[6] European Southern Observatory, Casilla 19001, Santiago 19, Chile
[7] LESIA, UMR 8109, Observatoire de Paris-Meudon, 5 place Jules Janssen, 92195 Meudon Cedex, France
[8] European Southern Observatory, Karl-Schwarzschild-Strasse 2, 85748 Garching bei München, Germany

ABSTRACT

Aims. The emission of warm dust dominates the mid-infrared spectra of active galactic nuclei (AGN). Only interferometric observations provide the necessary angular resolution to resolve the nuclear dust and to study its distribution and properties. The investigation of dust in AGN cores is hence one of the main science goals for the MID-infrared Interferometric instrument MIDI at the VLTI. As the first step, the feasibility of AGN observations was verified and the most promising sources for detailed studies were identified.
Methods. This was carried out in a "snapshot survey" with MIDI using Guaranteed Time Observations. In the survey, observations were attempted for 13 of the brightest AGN in the mid-infrared which are visible from Paranal.
Results. The results of the three brightest, best studied sources have been published in separate papers. Here we present the interferometric observations for the remaining 10, fainter AGN. For 8 of these, interferometric measurements could be carried out. Size estimates or limits on the spatial extent of the AGN-heated dust were derived from the interferometric data of 7 AGN. These indicate that the dust distributions are compact, with sizes on the order of a few parsec. The derived sizes roughly scale with the square root of the luminosity in the mid-infrared, $s \propto \sqrt{L_{\mathrm{MIR}}}$, with no clear distinction between type 1 and type 2 objects. This is in agreement with a model of nearly optically thick dust structures heated to $T \sim 300$ K. For three sources, the $10\,\mu$m feature due to silicates is tentatively detected either in emission or in absorption.
Conclusions. The faint AGN of the snapshot survey are at the sensitivity limit of observations with MIDI. Thus, the data set presented here provides a good insight into the observational difficulties and their implications for the observing strategy and data analysis. Based on the results for all AGN studied with MIDI so far, we conclude that in the mid-infrared the differences between individual galactic nuclei are greater than the generic differences between type 1 and type 2 objects.

Key words. galaxies: active – galaxies: nuclei – galaxies: Seyfert – techniques: interferometric

1. Introduction

In the standard model for active galactic nuclei (AGN), the central engine, consisting of a hot accretion disk around a supermassive black hole in the centre of a galaxy, is assumed to be surrounded by a geometrically thick torus of obscuring gas and dust. These dusty tori are held responsible for redistributing the optical and UV radiation from the hot accretion disk into the mid- and far-infrared as well as for the type 1 / type 2 dichotomy of AGN. In type 2 AGN, the torus is thought to be oriented edge-on so that it blocks the view towards the central engine; in type 1 AGN the torus is oriented face-on, allowing a direct view towards the central engine. The two types of AGN are hence considered to be intrinsically the same with any differences in their appearance arising from orientation effects (for a review,

see Antonucci 1993). However, this concept faces difficulties, as geometrically thick structures orbiting compact objects are expected to collaps to a thin disk within a few orbital periods (Krolik & Begelman 1988). Therefore, different theoretical concepts for the nuclear dust distribution and obscuring medium are currently being discussed. These include clumpy dusty tori – either supported by radiation pressure (Pier & Krolik 1992; Krolik 2007), by elastic collisions of the clouds (Krolik & Begelman 1988; Beckert & Duschl 2004) or by supernova explosions (Wada & Norman 2002; Schartmann et al. 2009) –, clumpy disk winds (e.g. Konigl & Kartje 1994; Elitzur & Shlosman 2006) or warped disks (e.g. Nayakshin 2005).

The dusty tori are too small to be significantly resolved with single dish telescopes in the thermal infrared ($\lambda \gtrsim 3\,\mu$m), even for 10 m class telescopes at the diffraction limit (with or without AO), which implies that the dust distributions are rather compact with sizes $\lesssim 10$ pc (e.g. Soifer et al. 2003; Horst et al. 2009). Until recently, the principle arguments for the existence of these tori were theoretical considerations and indirect observational

Table 1. Original list of targets for the MIDI SDT and GTO programme on AGN.

Galaxy name (1)	Alternative name (2)	RA (J2000) (3)	Dec (J2000) (4)	type (5)	D [Mpc] (6)	$\Delta(1\,\text{pc})$ [mas] (7)	Coudé guide star ψ [''] (8)	V [mag] (9)	$F_{11.9\,\mu m}$ [Jy] (10)
NGC 253		00 47 32.82	−25 17 19.6	HII	3	60	none		2.04
NGC 1068	M 77	02 42 40.70	−00 00 48.0	Sy 2	14	14	57	17	
NGC 1365		03 33 36.38	−36 08 25.7	**Sy 1.8**	**18**	**11**	**65**	**15**	**0.61**
IRAS 05189-2524	**LEDA 17155**	05 21 01.40	−25 21 45.3	**Sy 2**	**170**	**1.2**	none		**0.55**
MCG-05-23-016	**ESO 434-G040**	09 47 40.19	−30 56 56.4	**Sy 2**	**35**	**6**	**22**	**15**	**0.65**
Mrk 1239		09 52 19.10	−01 36 43.5	**Sy 1.5**	**80**	**2.5**	**54**	**15**	**0.64**
NGC 3256		10 27 51.24	−43 54 13.9	HII	40	5	32	15	0.55
NGC 3281		10 31 52.10	−34 51 13.3	**Sy 2**	**45**	**5**	**22**	**16**	**0.63**
NGC 3783		11 39 01.71	−37 44 19.0	Sy 1	40	5	45	17	0.59
NGC 4151		12 10 32.63	+39 24 20.7	**Sy 1.5**	**14**	**15**	none		
3C 273		12 29 06.70	+02 03 08.6	QSO	650	0.3	53	14	0.35
Centaurus A	NGC 5128	13 25 27.62	−43 01 08.8	FR I	4	54	44	13	1.22
IC 4329A	**ESO 445-G050**	13 49 19.35	−30 18 34.4	**Sy 1.2**	**65**	**3.1**	**58**	**17**	**0.35**
Mrk 463E		13 56 02.89	+18 22 18.2	Sy 1/2	200	1.0	none		0.34
Circinus	ESO 097-G013	14 13 09.95	−65 20 21.2	Sy 2	4	50	50	12	9.70
NGC 5506	**Mrk 1376**	14 13 14.88	−03 12 27.7	**Sy 1.9**	**25**	**8**	none		**0.91**
NGC 7469	**Mrk 1514**	23 03 15.68	+08 52 26.3	**Sy 1.2**	**65**	**3.1**	**13**	**15**	**0.41**
NGC 7582		23 18 23.63	−42 22 13.1	Sy 2	22	10	54	17	0.67

Notes: The columns are: (1) the name of the galaxy used in this paper; (2) an alternative name for the galaxy; (3) and (4) the coordinates of the nucleus used for the MIDI observations or, if no observations were carried out, the 2MASS coordinates; (5) the galaxy type (from NED); (6) the distance to Earth assuming $H_0 = 73\,\text{km s}^{-1}\,\text{Mpc}^{-1}$; (7) the angular size corresponding to 1 pc in the target; (8) the angular distance ψ and (9) the visual magnitude V of the best Coudé guide star (if present); (10) the flux at $11.9\,\mu m$ from Raban et al. 2008.

evidence such as the spectral energy distributions of AGN and the polarisation properties of Seyfert 2 nuclei.

The instrumental means to spatially resolve the nuclei of active galaxies at infrared wavelengths became available only with the advent of sufficiently sensitive interferometric instruments. One of these is the MID-infrared Interferometric instrument (MIDI) at the Very Large Telescope Interferometer (VLTI), located on Cerro Paranal in northern Chile and operated by the European Southern Observatory (ESO). Apart from two observations in the near-infrared with other interferomers, namely of the Seyfert 1 galaxy NGC 4151 with the Keck interferometer (Swain et al. 2003) and of the Seyfert 2 galaxy NGC 1068 with the VINCI instrument also at the VLTI (Wittkowski et al. 2004), MIDI is currently the only interferometer to successfully observe active galactic nuclei in the infrared wavelength range.

The first AGN to be targeted by MIDI was the brightest AGN in the mid-infrared, NGC 1068. These observations were carried out during the Science Demonstration Time (SDT) of the instrument and succeded in resolved the nuclear dust emission (Jaffe et al. 2004; Poncelet et al. 2006). This demonstrated the great potential of MIDI for the investigation of AGN. Further MIDI observations of NGC 1068 were subsequently carried out in Open Time (Raban et al. 2009).

Using mainly Guaranteed Time Observations (GTO), the two next brightest AGN, the radio galaxy Centaurus A and the Circinus galaxy, a Seyfert 2 galaxy, were studied with MIDI. The results were published in Meisenheimer et al. (2007) and Tristram et al. (2007) respectively. The MIDI observations of NGC 1068 and the Circinus galaxy have directly confirmed that, indeed, compact AGN heated dust structures on the scale of a few parsecs exist in Seyfert 2 galaxies and that it is possible to determine their size as well as their orientations with respect to the source axis (Jaffe et al. 2004; Poncelet et al. 2006; Tristram et al. 2007 and Raban et al. 2009). On the other hand, the mid-infrared flux from Centaurus A is dominated by an unresolved core (most likely the high-frequency tail of the radio

core) which is surrounded by a low luminosity "dust disk" of about 0.6 pc diameter (Meisenheimer et al. 2007).

Apart from these three well studied sources, all other AGN which can potentially be observed with MIDI are less bright in the mid-infrared and are close to, or at, the sensitivity limit of MIDI. In order to determine which AGN are suitable for further study with MIDI, a snapshot survey of potential targets was carried out during GTO. In this survey, each source on the target list was to be observed at least once in order to test for the feasibility of MIDI observations as well as to obtain first estimates for the basic mid-infrared properties of the target sources. The results of this survey are presented in this paper.

The paper is organised as follows: Sect. 2 describes the original target list together with the properties of the sources; in Sect. 3, the general observational strategy as well as the general challenges for the data reduction are presented; in Sect. 4, the results for the individual sources are discussed, while in Sect. 5 a summary of the observational results is given. The discussion and the conclusions are found in Sects. 6 and 7 respectively. A more detailed discussion of the observations and the data reduction procedures for the individual sources is given in Appendix A.

2. Target list

The original list of targets for both the GTO and the SDT (see Table 1) contains those 16 active galaxies from Raban et al. (2008), plus NGC 1068, which are well observable from Cerro Paranal (Dec < +25°) and which were thought to be bright enough for MIDI observations (unresolved core flux $F_{\text{core}} \gtrsim 0.35\,\text{Jy}$). Additionally, the prototypical Seyfert 1 galaxy NGC 4151 was included in the list. Because of its northerly position at Dec = +39° 24′, the latter does not rise more than 26° (corresponding to an airmass of 2.3) above the horizon at the location of the VLTI (24° 40′ S). Despite the difficulty of observing it from Paranal, it was also included in the list of GTO

Table 2. Overview of the observations and observation attempts for the sources from Table 1.

Galaxy name (1)	First / last observation (2)	Programme number (3)	Coudé guiding (4)	Fringe tracks (5)	Result of the MIDI observations (6)
NGC 253	observed by S. Hönig (no fringes detected)				
NGC 1068	2003 Jun 15	060.A-9224(A)[a]	nucleus	9[b]	well resolved (Raban et al. 2009)
* **NGC 1365**	**2006 Sep 11**	**077.B-0026(B)**	**nucleus**	**7**	**partially resolved (possibly elongated)**
* **IRAS 05189-2524**	**2006 Sep 11**	**077.B-0026(B)**	**nucleus**	**1**	**faint fringe detection only**
* **MCG-05-23-016**	**2005 Dec 19**	**076.B-0038(A)**	**star**	**1**[b]	**partially resolved**
* **Mrk 1239**	**2005 Dec 19**	**076.B-0038(A)**	**nucleus**	**2**[b]	**essentially unresolved**
NGC 3256					not yet observed
* **NGC 3281**	**2007 Feb 07**	**078.B-0031(A)**	**nucleus**	**none**	**no AO correction possible using the nucleus**
NGC 3783	see Beckert et al. (2008)				partially resolved
* **NGC 4151**	**2007 Feb 07**	**078.B-0031(A)**	**nucleus**	**2**	**well resolved**
* **3C 273**	**2007 Feb 07**	**078.B-0031(A)**	**nucleus**	**4**	**possibly resolved**
Centaurus A	2005 Mar 01	074.B-0213(B)	star	5[b]	partially resolved (Meisenheimer et al. 2007)
* **IC 4329A**	**2007 Feb 07**	**078.B-0031(A)**	**nucleus**	**2**[b]	**unresolved**
Mrk 463E					not yet observed
Circinus	2004 Jun 03	060.A-9224(A)[a]	star	22[b]	well resolved (Tristram et al. 2007)
* **NGC 5506**	**2007 Feb 07**	**078.B-0031(A)**	**nucleus**	**none**	**no AO correction possible using the nucleus**
* **NGC 7469**	**2006 Sep 11**	**077.B-0026(B)**	**nucleus**	**3**	**well resolved**
NGC 7582	observed by S. Hönig (no fringes detected)				

[a] The first observations of NGC 1068 and the Circinus galaxy were carried out in SDT.

[b] In the meantime, more observations than those listed here have been obtained for several of the original SDT and GTO targets in Open Time.

Notes: The objects of the snapshot survey discussed in this paper are highlighted by boldface and marked by asterisks. The columns are: (1) the name of the galaxy (repeated from Table 1); (2) the date and (3) ESO programme number of the first successful observation or the last unsuccessful observation attempt; (4) the type of Coudé guiding used for the observations; (5) the number of successful fringe tracks obtained in SDT and GTO (without judgement on whether the data are useful or not) and (6) the result of the MIDI observations.

targets due to (1) its importance as the nearest and brightest type 1 AGN and of (2) it being one of the two AGN observed by other interferometers.

In preparation for the MIDI observations, high resolution imaging was carried out for most of the AGN on the target list in the near-infrared with NACO, the adaptive optics assisted multi mode instrument of the Very Large Telescope (Rousset et al. 2003; Lenzen et al. 2003), and in the mid-infrared with TIMMI2, the Thermal Infrared Multi-Mode Instrument 2 (Käufl et al. 2003). Essentially, all nuclei remain unresolved both in the near- and mid-infrared. The results of the investigation with TIMMI2 were published in Raban et al. (2008); those of the investigation with NACO will be presented in Prieto et al. (in preparation). The photometric values of the targets at $11.9\,\mu$m from Raban et al. (2008), for aperture sizes ranging from 1.2 arcsec to 2.6 arcsec, are listed in the last column of Table 1.

As the observations progressed, several galaxies from the original target list were released from the GTO protection without being observed. NGC 253, NGC 3256, NGC 3783, Mrk 463E, and NGC 7582 are among these galaxies released. For some of these sources, observations were attempted by other authors: NGC 3783 was successfully observed in Open Time by Beckert et al. (2008); for NGC 253 and NGC 7582 no interferometric signal could be detected (Hönig, private comm.).

A summary of the observations and results for all the sources from the original target list is given in Table 2. The ten objects discussed in detail in this paper, that is, the sources of the snapshot survey, are highlighted by boldface and marked by an asterisk.

## 3. Observations and data reduction

3.1. The MIDI instrument

MIDI is a two beam Michelson type interferometer producing dispersed fringes in the N band over a wavelength range from 8 to $13\,\mu$m (Leinert et al. 2003). For our observations, the light of two of the 8.2 m unit telescopes (UTs) was combined at any one time. The incoming wavefronts from the two telescopes were corrected using the Multi Application Curvature Adaptive Optics system (MACAO, Arsenault et al. 2003). All of the AGN in the snapshot survey were observed in high sensitivity (HIGH-SENS) mode and with low spectral resolution ($\lambda/\delta\lambda \approx 30$). This mode uses a NaCl prism after the beam combiner. As the main goal of this survey was to test for the feasibility of MIDI observations, the two shortest baselines, UT2 – UT3 and UT3 – UT4, were used for most of the observing runs to obtain the highest possible correlated fluxes. An observation run planned for 2007 May 05 with the longer UT2 – UT4 baseline was completely lost due to bad weather conditions.

3.2. Observing sequence

We now briefly discuss the observing sequence and data reduction, while putting a special emphasis on the challenges in the context of sources at the detection limit of MIDI and the VLTI. A detailed description of the observing sequence can be found in Tristram (2007). The peculiarities of the observations and data reduction for the individual objects are discussed in Appendix A.

After the telescopes have been pointed at the source, the AO system, MACAO, must close the loop on its reference source. This can be either the nucleus of the source itself, or – if available – on a Coudé guide star with $V < 17$ mag and within 57 arcsec of the source. For most of the sources this correction used the
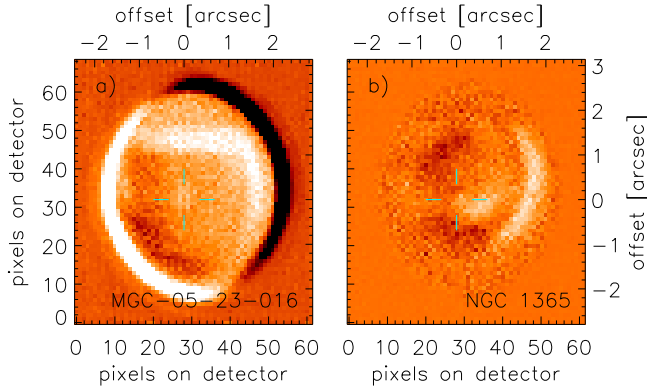
Fig. 1. Final acquisition images of **a)** MCG-05-23-016 (observed 2005 Dec 19) and **b)** NGC 1365 (observed 2006 Sep 11). Both sources have a total flux of about $F \sim 0.5$ Jy and NDIT = 16 000 was used. The sources are barely recognisable due to the high number of frames. The residual background from the VLTI tunnels is much stronger than the sources. A less even background would completely prevent a detection of the source.

nucleus itself (see Table 2). In several cases, this turned out to be at the limit of the abilities of the MACAO system resulting in difficulties obtaining a stable correction. This was especially true for poor seeing conditions.

The difficulty is largely that the AO corrections are determined in the optical where the nuclei may be faint due to obscuration; in addition, the optical cores of the host galaxies are spatially extended. This issue will be further discussed in Sect. 5.

The next step in the observing sequence is to align the beams from the two telescopes. This uses acquisition images made with each telescope. For our observations, the number of individual exposures had to be increased significantly from the standard value of NDIT = 1000 to, for instance, NDIT = 16 000 in order to make the source visible against the residual background. Even for such increased integration times, several of our sources were barely discernible against the residual background, as can be seen from Fig. 1.

Since our observations in September 2006, the VLTI infrared field-stabiliser IRIS (InfraRed Image Sensor, Gitton et al. 2004) has been available. The purpose of IRIS is to stabilise the field of the beams by measuring the low-frequency tip-tilt directly in the VLTI laboratory, where MIDI is located. For sources bright enough in the near-infrared ($K < 14$ mag), IRIS guarantees the correct alignment of the beams during the observations. If one trusts that a proper alignment of the beams in IRIS also produces a proper alignment of the beams in MIDI[1], no acquisition images with MIDI itself are necessary. Nevertheless, we continued to record acquisition images in later observing runs in order to verify the correct overlap of the beams and the quality of the source image with respect to the background emission. Only for two of the sources observed on 2007 Feb 07 (3C 273 and IC 4329A) and for the last observation of NGC 1365 on 2007 Nov 24, no acquisition images were obtained.

After the beams are aligned, the beamsplitter, a 0.52 arcsec wide slit and the prism are inserted into the light path and a so-

called *fringe search* is performed in order to determine the position of the zero optical path difference (OPD) between the two beams. If an interferometric signal was detected in the fringe search, the path difference is stabilised (except for a small modulation) at or near zero OPD, while the spectrally dispersed interferometric signal is continuously recorded in order to increase the signal to noise ratio. This is the so-called *fringe track*. Because the strong background emission in the mid-infrared is uncorrelated, it can be effectively removed during the data reduction process by high pass filtering of the modulated fringe signal in delay and frequency space. Therefore, no chopping needs to be performed during the interferometric measurements and a more stable AO correction is achieved. All of our observations were carried out in "offset tracking" mode with the OPD stabilised at $50\,\mu$m from zero OPD. This tracking mode is advantageous for sky removal using a high pass filter in frequency space, as the signal is always modulated in wavelength; at zero OPD this is not the case.

Finally, photometric data, that is, single dish spectra, are recorded using only one telescope at a time for an otherwise identical optical set-up. As for the aquisition, chopping is used to suppress the background.

The entire procedure of acquisition, fringe search, fringe track and photometry is repeated for the calibrator star to obtain a single calibrated visibility point.

3.3. Data reduction

The data reduction was performed with EWS (Expert Work Station[2], Version 1.7), a data reduction package based on the coherent data reduction method. A detailed description of EWS is found in Jaffe (2004). The parameters for the EWS data reduction were `smooth = 10`, `gsmooth = 20`, `dave = 1` and `nophot = 1`, the last parameter meaning that we chose to directly calibrate the correlated fluxes without using the photometric fluxes. The calibration used the database of stellar spectra from Roy van Boekel (private comm.).

During the data reduction process, we noticed a secular drift of the position of the dispersed signal on the MIDI detector. For data obtained in November 2007, the shift had become so large ($\sim$3 pixels = 0.26 arcsec) that the dispersed fringes and the spectra of the photometry were moving outside the standard EWS mask. For this reason, we constructed a separate mask for every observing run, taking into account the position and width in spatial direction of the spectra. Additionally, the sky bands used for the determination of the photometry were adjusted according to the new mask position.

The results of the data reduction process are the spectrally dispersed correlated flux $F_{cor}(\lambda)$ (from the interferometric measurement), the total flux spectrum $F_{tot}(\lambda)$ (from the photometric measurement, corresponding to an aperture of 0.52×1.1 arcsec^2) and the visibility spectrum $V(\lambda)$ (derived from both the interferometric and the photometric data). For an ideal measurement, $V = F_{cor}/F_{tot}$. In practice, however, this is often not the case (for a detailed discussion, we refer to Tristram 2007).

For sources as weak as those discussed here, the statistical errors determined by EWS have to be considered with caution. Especially, the photometry can have unrealistically large errors. These come from the variations of the flux induced by the background residual. Extremely large errors were simply truncated corresponding to a relative error of 90 %. The large errors of the

---

[1] The position of the photocentre of the source may, however, depend on the wavelength. Also, at high airmasses, the wavelength dependency of the atmospheric refraction leads to different apparent positions of the source in the near and mid-infrared which might lead to slightly different positions in MIDI and IRIS.

[2] The software package "MIA+EWS" is available for download at http://www.strw.leidenuniv.nl/~nevec/MIDI/index.html

photometry propagate into the visibility, but not into the correlated flux due to its direct calibration. The latter seems to have rather too small errors.

Due to the low quality or the incompleteness of several data sets, especially the photometric components, special data reduction procedures had to be applied to obtain meaningful results. The photometric data were completed or their quality improved by mainly using the three following methods: (1) where no photometry observations were carried out at all, photometry data obtained in conjunction with another fringe track were used to complete the data set; (2) if only one of the two photometric measurements contains a useful signal (e.g. if there was no AO correction for one of the two telescopes during chopping), only that photometry was used to determine the total flux and (3) for strong background residuals, only those portions of the photometry integration where the background residual is relatively flat were used for the determination of the total flux spectrum. A description of which method and which additional steps were carried out for each of the individual sources is given in Appendix A.

3.4. Compilation of comparison spectra

In order to check whether the MIDI data are reasonable and in order to be able to interpret the correlated fluxes where no or only a questionable total flux spectrum was observed, additional mid-infrared spectra were compiled. Preference was given to data obtained with the highest angular resolution. For lack of alternative (no high resolution ground-based spectra available), Spitzer spectra were retrieved from the archive for several sources. The Spitzer spectra used for our comparison were observed with the Short-Low (SL, $\lambda/\delta\lambda \approx 60-120$) module of IRS, the InfraRed Spectrograph (Houck et al. 2004) on the Spitzer Space Telescope, in staring mode. The nuclear spectra directly delivered by the pipeline, version S15.3, were used, without applying further correction factors. Note that a direct comparison of the Spitzer IRS spectra with MIDI data is only possible with reservations due to the large difference in the apertures of the two instruments (3.6×6.0 arcsec^2 for IRS and 0.5×1.1 arcsec^2 for the total flux in MIDI). This is especially the case for sources also harbouring a nuclear starburst and thus displaying extended emission in the infrared, such as NGC 7469 (see Sect. 4.7). The Spitzer spectra thus have to be seen as upper limits to the ones measured by MIDI.

4. Results

The results of the measurements are presented for those seven sources where useful data could be obtained. These are NGC 1365, MCG-05-23-016, Mrk 1239, NGC 4151, 3C 273, IC 4329A and NGC 7469. For the remaining three sources of the snapshot survey, no useful data could be obtained: for NGC 3281 and NGC 5506, no measurements with MIDI were possible at all, because no stable AO correction could be achieved with MACAO using the extended nuclei for guiding. For IRAS 05189-2524 the interferometric signal was too weak for fringe tracking (see Appendix A.2).

For those sources where both an interferometric measurement as well as a proper measurement of the total flux spectrum was carried out with MIDI, a very crude estimate or a limit on the size of the emission region can be derived assuming a Gaussian brightness distribution. A Gaussian flux distribution is the simplest and most general initial guess for the shape of the source. Even if the true shape of the flux distribution differs from

a Gaussian, it provides us with a correct scale of the spatial extent of the source.

The full width at half maximum $FWHM(\lambda)$ of the Gaussian brightness distribution is related to the visibility $V(\lambda)$ and the projected baseline length BL by

$$FWHM(\lambda) = \frac{\lambda}{BL} \cdot \frac{2}{\pi} \sqrt{-\ln 2 \cdot \ln V(\lambda)}. \qquad (1)$$

By definition, $FWHM(\lambda) = 0$ when $V(\lambda) = 1$[3]. Because of the nonlinear dependency of the $FWHM$ on the visibility in Eq. 1, the upper and lower limits on the $FWHM$ were calculated directly from the upper and lower limits of the visibility.
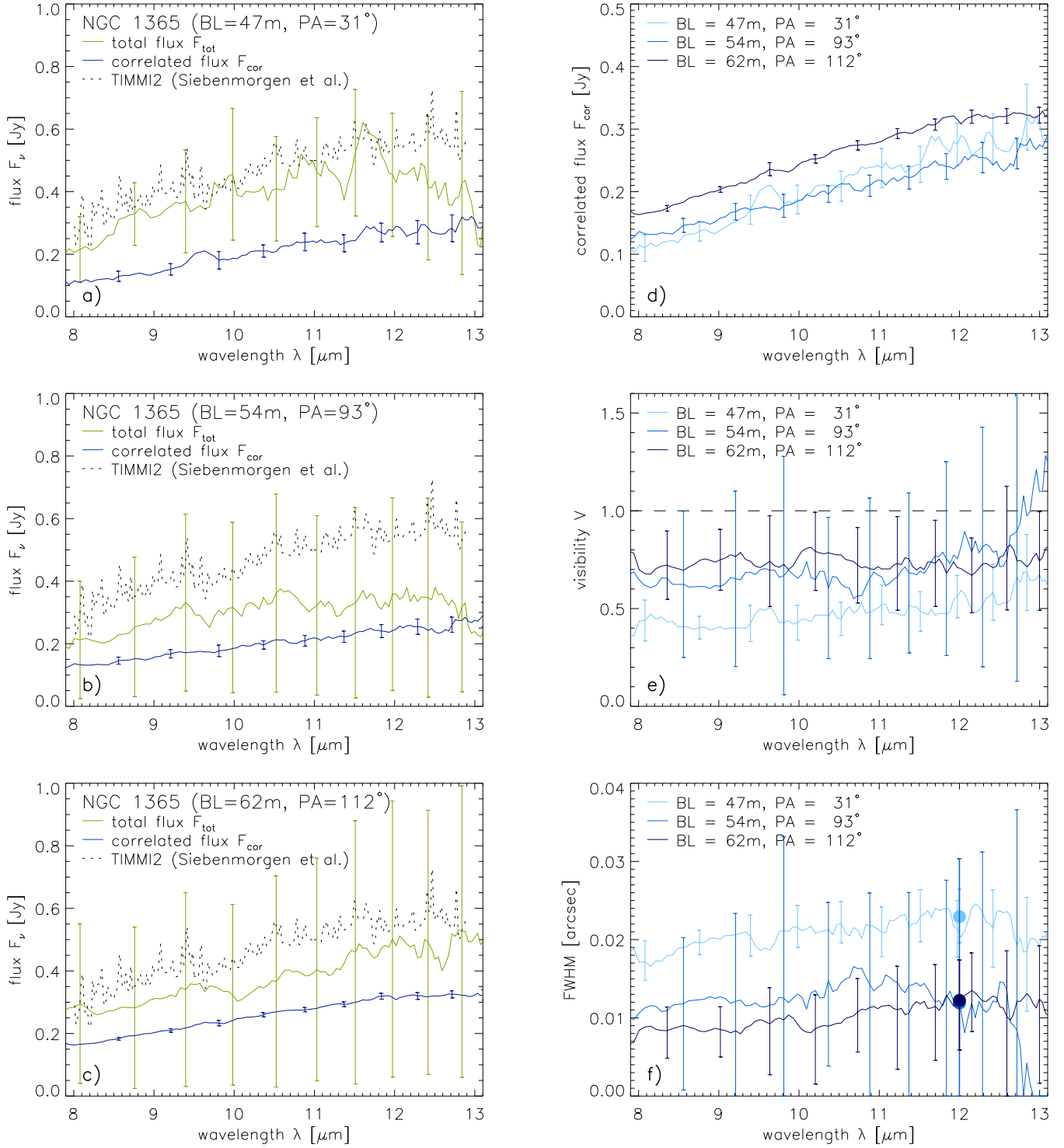
4.1. NGC 1365

The large, barred spiral galaxy NGC 1365 is located at a distance of 18.3 ± 3.3 Mpc (1 arcsec = 90 pc, Silbermann et al. 1999) in the Fornax cluster of galaxies. The Seyfert type of this galaxy is variable. This is seen as prime evidence for a clumpy torus (e.g. Risaliti et al. 2009, and references therein). An extensive overview of this galaxy is found in Lindblad (1999). In the mid-infrared, TIMMI2 data show that the nucleus is surrounded by 7 individual sources within 20 arcsec from the nucleus (Galliano et al. 2005; Raban et al. 2008), which are interpreted as embedded young star clusters. The nuclear source itself shows a slight extension in E-W direction in the data from Galliano et al., but this extension has not been confirmed by Raban et al. (2008). A TIMMI2 spectrum of the nucleus is presented in Siebenmorgen et al. (2004). It is featureless and flat, without any evidence of silicate absorption or emission.

The MIDI data are presented in Fig. 2. In the left column, the correlated and total flux spectra for the three different baseline lengths and orientations at which the source was observed are shown together with the TIMMI2 spectrum from Siebenmorgen et al. (2004). Neither the total nor the correlated fluxes show indication of a silicate feature, consistent with the featureless TIMMI2 spectrum. Our total flux spectra show a continuous increase of the spectrum from ~0.25 Jy at 8 μm to ~0.50 Jy at 13 μm, except for the second measurement (Fig. 2b), where up to 30 % lower flux values were measured. The MIDI spectra thus seem to be slightly lower than the spectrum obtained with TIMMI2. Nevertheless, all of the MIDI total flux spectra are consistent with each other and with the TIMMI2 spectrum when taking into account their large uncertainties. These uncertainties are caused by the residuals of the background subtraction which are especially strong for the second measurement. We consider the variations among our measurements as an indication of the applicability of our data reduction methods and of the true uncertainty in the determination of the total flux. The correlated fluxes on the other hand rise from ~0.15 Jy at 8 μm to ~0.30 Jy at 13 μm and are hence below the level of the total flux measurements ($F_{\text{cor}} < F_{\text{tot}}$). About 30 to 40 % of the nuclear mid-infrared flux is resolved by our interferometric set-up.

A comparison of the three correlated flux spectra and the corresponding visibility spectra is given in Fig. 2d and e respectively. Taking into account that a longer baseline length means a higher spatial resolution, the source appears more extended along $PA = 31°$ than along $PA = 112°$: the correlated flux at $PA = 31°$ tends to be slightly lower than that at $PA = 112°$, despite the longer baseline and the consequently higher spatial

---

[3] Theoretically, $V(\lambda)$ cannot be greater than 1. Practically, however, it is not uncommon to obtain $V(\lambda) \geq 1$ simply due to the error of the measurements. For such cases we set $FWHM = 0$.

Fig. 2. Correlated and total flux spectra, visibilities and size estimates for the three interferometric measurements of NGC 1365. For sake of clarity, the error bars for the MIDI data are given for every tenth wavelength bin. In *the left column*, panels **a)**–**c)**, the correlated (blue) and total (green) flux spectra are displayed for each of the three baseline orientations. For comparison, the TIMMI2 spectrum from Siebenmorgen et al. (2004) is also shown (dotted line). In panel **d)** the three measurements of the correlated flux are shown together in a single plot. Panels **e)** and **f)** show the visibility spectra and the derived *FWHM* of a corresponding Gaussian flux distribution, respectively. The size estimates at $12\,\mu$m used in Sect. 6.2 are indicated in panel **f)** by filled circles.
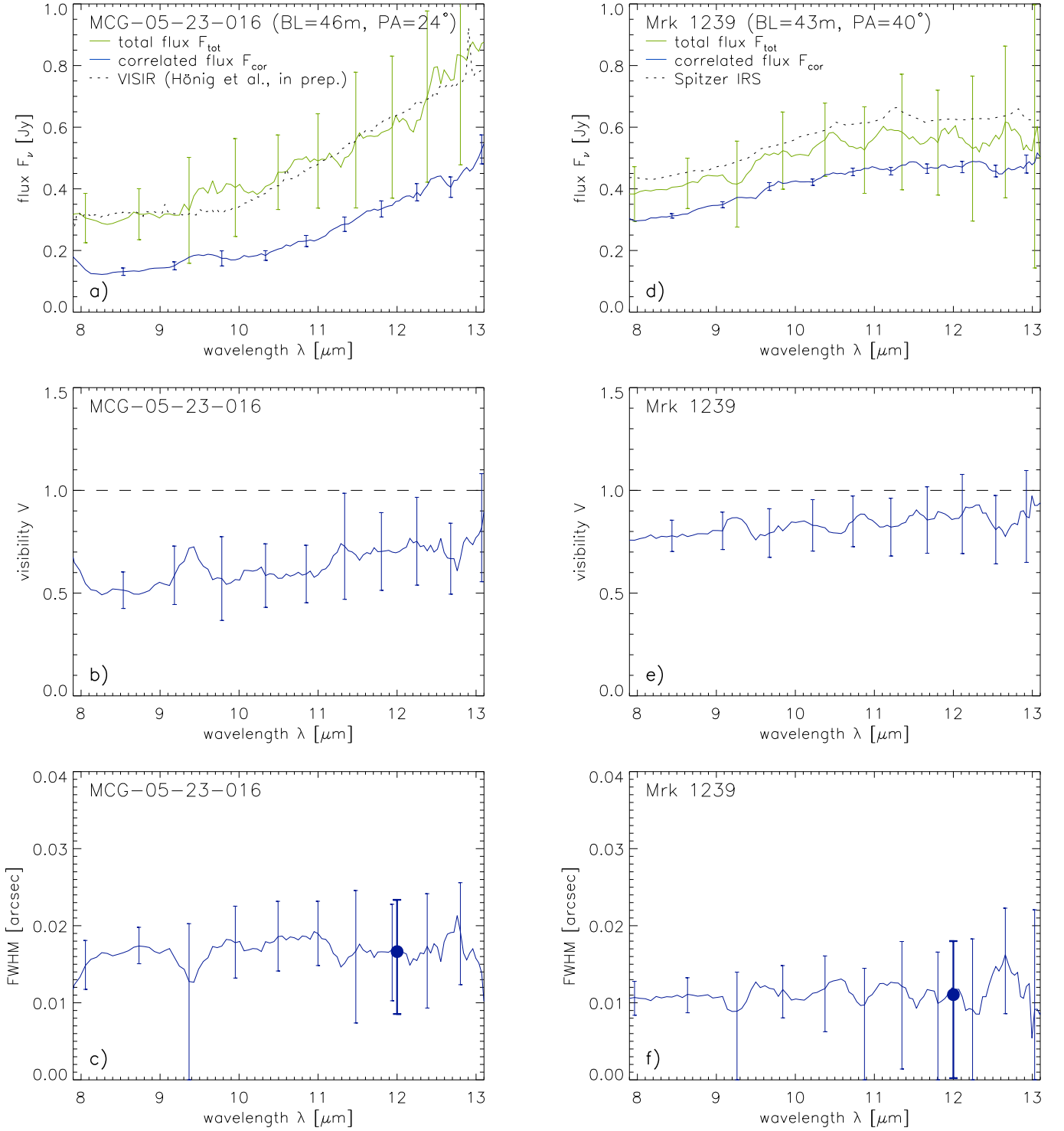
Fig. 3. Results of the interferometric measurements with MIDI for MCG-05-23-016 (*left column*) and for Mrk 1239 (*right column*). In the first row, the correlated (blue) and the total (green) flux spectra are displayed. For comparison, the VISIR spectrum for MCG-05-23-016 from Hönig et al. (in preparation a) and the Spitzer spectrum for Mrk 1239 are also plotted (dotted lines). In the second row, the visibilities are shown. The last row shows the *FWHM* of a corresponding Gaussian flux distribution. The size estimates at $12\,\mu$m (see Sect. 6.2) are indicated by filled circles. For the sake of clarity, the errors of the MIDI data are only indicated for every tenth wavelength bin.

resolution for the measurement at $PA = 112°$. The same conclusion follows from the visibilities: the two visibilities at $PA = 93°$ and $112°$ are still consistent with an unresolved source (i.e. with $V = 1$), while the visibility at $PA = 31°$ indicates that the source is partially resolved.

The angular sizes derived from the visibilities according to Eq. 1 are displayed in Fig. 2f. The assumed Gaussian brightness distribution has an angular extent between 5 and 30 mas. Like the correlated fluxes or the visibilities, the size estimates show evidence for an asymmetry with a larger extent of the source ($\sim$20 mas) along $PA = 31°$ and a smaller size ($\sim$10 mas) along $PA = 112°$. At the distance of NGC 1365, 20 mas correspond to 2 pc, which sets a strong limit on the global size of the distribution of warm dust in the nucleus of this galaxy. We note that, if our tentative detection of an elongated structure along $PA \sim 31°$ can be confirmed, it would not agree with the E-W elongation claimed by Galliano et al. (2005). It would, however, lie more or less perpendicular to the ionisation cone at $PA \sim 130°$ (Wilson & Tsvetanov 1994; Hjelm & Lindblad 1996) and the radio "jet" at $PA = 125°$ (Kinney et al. 2000).

4.2. MCG-05-23-016

MCG-05-23-016 (ESO 434-G40) is a lenticular Seyfert 2 galaxy at a distance of 35 Mpc ($v_{hel} = 2544 \pm 12$ km s^{-1}, Wegner et al. 2003; 1 arcsec = 170 pc), which has been studied mostly for its X-ray emission (e.g. Balestra et al. 2004; Mattson & Weaver 2004). Its mid-infrared spectrum is characteristic of this type of nucleus, rising strongly towards longer wavelengths and it displays a very shallow silicate absorption feature (see also Frogel et al. 1982).

The data obtained with MIDI are shown in the left column of Fig. 3. The values measured for the total flux are on the order of 0.3 Jy from 8 to 10 μm and then continuously increase to 0.8 Jy at 13 μm. Hence, the spectrum is in excellent agreement with the VISIR spectrum presented in Hönig et al. (in preparation a) and with our TIMMI2 photometry: 0.65 ± 0.10 Jy at 11.9 μm. We are confident that the total flux values measured by MIDI are accurate for this galaxy. The correlated flux is considerably lower than the total flux ($F_{cor} < F_{tot}$), indicating that the emitter in the mid-infrared is partially resolved: roughly between 30 % (at 13 μm) and 50 % (at 8 μm) of the nuclear flux are resolved out by our interferometric measurement. This is also reflected by the visibility which is on the order of 50 to 70 % (see Fig. 3b).

Assuming a Gaussian flux distribution, an upper limit for the emission region in MCG-05-23-016 can be derived: at $\lambda = 12$ μm it has a size of less than 23 mas, which corresponds to less than 4.0 pc at the distance of this galaxy (see thick error bar at $\lambda = 12$ μm in Fig. 3b). From the fact that this source is slightly resolved, we similarly deduce a lower limit for the size of the emission region, which is roughly 9 mas and corresponds to 1.5 pc in MCG-05-23-016.

4.3. Mrk 1239

Mrk 1239 is a narrow-line Seyfert 1 (NLS1) galaxy located at a distance of about 80 Mpc ($v_{hel} = 5747$ km s^{-1}, Beers et al. 1995; 1 arcsec = 380 pc). Its unresolved near-infrared emission shows a strong bump at 2.2 μm which is interpreted as very hot dust near its sublimation temperature ($T \sim 1200$ K), very likely located both in the upper layers of the torus and close to the apex of the polar scattering region (Rodríguez-Ardila & Mazzalay 2006). While the source appears unresolved with a flux of
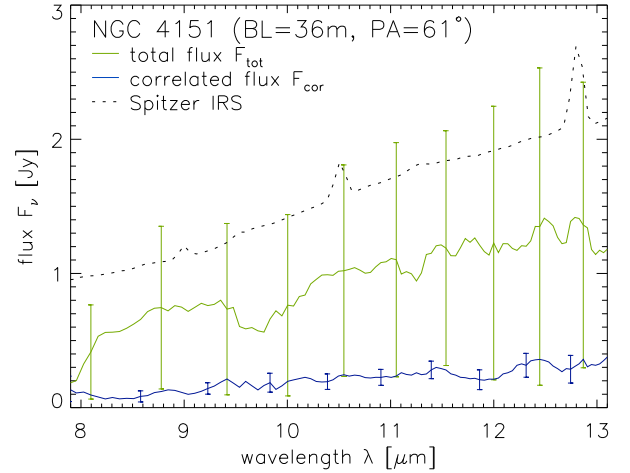
Fig. 4. Correlated (blue) and total (green) flux spectra for the nucleus of NGC 4151. Also plotted is the spectrum obtained with Spitzer (dotted line) which clearly shows the [Ar III], [S IV] and [Ne II] emission lines at 9.0 μm, 10.5 μm and 12.8 μm respectively (cf. also Fig. 1 in Weedman et al. 2005). For the sake of clarity, the errors of the MIDI data are only indicated every tenth wavelength bin.

0.64 ± 0.10 Jy in the TIMMI2 image at 11.9 μm (Raban et al. 2008), Gorjian et al. (2004) detected an approximately 1 arcsec long extension from the nucleus to the northwest.

The correlated and total flux spectra, the visibility spectrum as well as the derived sizes for a Gaussian brightness distribution are displayed in the right column of Fig. 3, panels d)–f), respectively. The MIDI total flux spectrum is rising from 0.4 to 0.6 Jy. It is slightly lower but still consistent with the Spitzer spectrum as well as with the 0.64 Jy measured with TIMMI2 at 11.9 μm (cf. Table 1). The overall shapes of the MIDI and Spitzer spectra agree well: they both exhibit the silicate feature in emission (slightly convex shape of the spectra). The good agreement between the MIDI and Spitzer spectra despite the difference in apertures can be explained by the nature of Mrk 1239 as a Seyfert 1 galaxy without evidence of a starburst, thus implying a compact, solely AGN dominated emission region in the mid-infrared. The correlated flux spectrum is slightly lower than the total flux spectrum, although they are consistent with each other within the errors. As a consequence, the mid-infrared source in this nucleus is only slightly resolved, if at all. This can also be seen from the visibility, which is larger than 80 %, with errors on the order of 20 %. From the upper limit on the full width at half maximum of an assumed Gaussian flux distribution we conclude that the mid-infrared source in Mrk 1239 most likely has a size of less than $\sim$18 mas, that is, less than 7 pc.

4.4. NGC 4151

At a distance of 13.6 Mpc ($v_{hel} = 997 \pm 3$ km s^{-1}, Pedlar et al. 1992; 1 arcsec = 65 pc), NGC 4151 hosts the closest and brightest ($F_N = 1.4$ Jy, Radomski et al. 2003) Seyfert 1 nucleus. It has been extensively studied at all wavelengths. High resolution mid-infrared observations are presented in Neugebauer et al. (1990), Radomski et al. (2003) and Soifer et al. (2003). They show that $\leq$70 % of the total mid-infrared flux comes from a core component with a size of $\leq$10 pc, while the rest originates in extended emission from dust in the narrow line region.
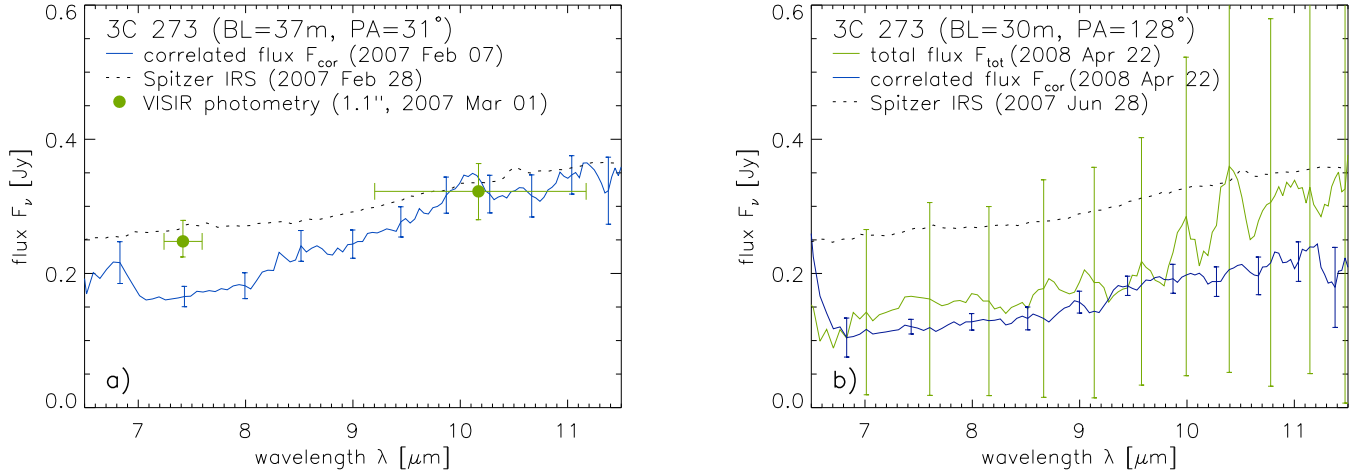
Fig. 5. Results for 3C 273. Panel **a)** shows the spectrum of the correlated flux measured with MIDI on 2007 Feb 07 (blue line) compared to the intermediate band photometry with VISIR (green dots) and a Spitzer spectrum from 2007 Feb 28 (dotted line). For the VISIR data, the error bars in the wavelength direction correspond to the width of the filter at half of the maximum transmission. In panel **b)**, the MIDI measurements from 2008 Apr 22 are plotted together with a Spitzer spectrum from 2007 Jun 28. The Spitzer spectrum in panel **b)** was observed four months after the one displayed in panel **a)**, nevertheless both are almost identical. Due to the relatively high redshift of this source ($z = 0.158$), the wavelength range plotted was shifted. For the sake of clarity, the errors of the MIDI data are only indicated every tenth wavelength bin.

Observations with the Keck Interferometer have shown that the near-infrared emission of the nucleus is very compact ($\leq$0.1 pc, Swain et al. 2003).

The results of the MIDI observations of NGC 4151 from February 2007 are displayed in Fig. 4 together with the Spitzer spectrum. The total flux spectrum rises from ~0.5 Jy at 8 μm to ~1.3 Jy at 13 μm. Its general shape agrees with the shape of the Spitzer spectrum, although it is lower by a factor of 30 to 50 %. None of the smaller scale variations can be trusted and the decrease of flux below 8.2 and around 9.7 μm is due to an inadequate removal of the absorption caused by water and ozone in the Earth's atmosphere during calibration, especially at the high airmass at which this source was observed. The Spitzer and the MIDI spectra are consistent with the flux being distributed in an unresolved "core" and an extended component as described by Radomski et al. (2003) when accounting for the difference in the apertures. The correlated flux spectrum is even lower, on a level between 0.1 and 0.3 Jy, implying that the mid-infrared source is clearly resolved. With a baseline length of $BL = 35.8$ m and assuming a visibility of $V = F_{cor}/F_{tot} \sim 20$ % at $\lambda \sim 12$ μm, we obtain a size of the emission region on the order of 45 mas, which is ~3 pc at the distance of NGC 4151. That the emission appears to be resolved on such scales shows that most of the mid-infrared emission is of thermal origin. The size derived here is significantly smaller than the 10 pc from Neugebauer et al. (1990) but well above the estimated inner radius of the torus, $r_{inner} = 0.04$ pc (Minezaki et al. 2004). A full analysis of the MIDI data of this source will be given in Burtscher et al. in preparation.

4.5. 3C 273

3C 273 (PG 1226+023) was the first quasar to be discovered (Schmidt 1963). As it is the brightest object of its kind and because it exhibits a one-sided jet which is visible from the radio regime to γ-rays, it is one of the best observed and studied AGN. The quasar is located at a redshift of $z = 0.158$, which corre-

sponds to a distance of 650 Mpc (1 arcsec = 3.1 kpc, Schmidt 1963). A detailed review of the source is given by Courvoisier (1998).

The results of our measurements are shown in Fig. 5. Due to the relatively high redshift, the restframe wavelengths probed by MIDI are between 6.5 and 11.5 μm. For the first measurement (panel a)), no total flux measurement could be obtained; only intermediate band photometry could be carried out with VISIR 21 days after the interferometric observations (see Appendix A.6). For the second measurement (panel b)), the total flux spectrum has very large errors. Therefore the interferometric data are compared to Spitzer spectra. These were obtained on two different dates: 2007 Feb 28 (one day before the observations with VISIR) and 2007 Jun 28. Both Spitzer spectra are almost identical. They are well suited for comparison to the MIDI data because of the pointlike nature of the nucleus in 3C 273: neither in our VISIR imaging (cf. Appendix A.6) nor in our observations with TIMMI2 (Raban et al. 2008) are there signs for extended emission. Furthermore, the VISIR measurements are consistent with the Spitzer spectra, as are the TIMMI2 measurements. We interpret this as an indication that the total flux measured by MIDI in 2008 underestimates the true flux of the source.

The correlated fluxes both rise between 6.5 and 11.5 μm. This is mainly due to the silicate feature in emission, which has its peak at 11 μm when looking at the entire mid-infrared spectrum (cf. Fig. 1 in Hao et al. 2005). The measurement on 2007 Feb 07 has a relatively steep, increasing spectrum and flux values consistent with the Spitzer spectrum at the long wavelength end. The source appears to be only resolved to a minor fraction and only at shorter wavelengths. The correlated fluxes from 2008 Apr 22, on the other hand, follow the Spitzer spectrum at levels of 50 to 60 %. It thus seems that up to half of the flux of the source is resolved, and this despite the shorter baseline length and thus smaller spatial resolution. The difference between the correlated fluxes may have two causes: (1) the difference in baselines or (2) the variability of the source. The two interferometric measurements were taken with almost perpendic-
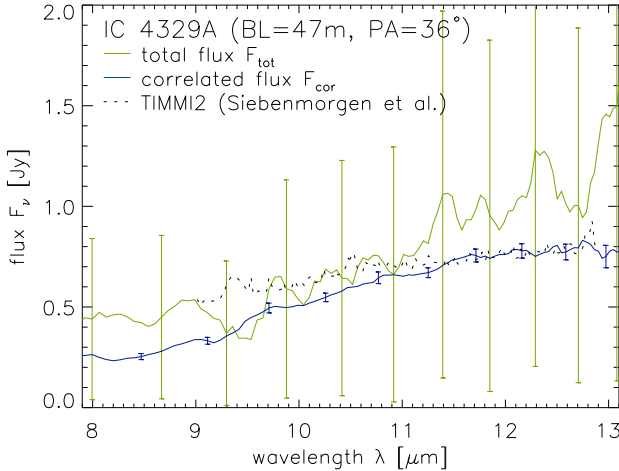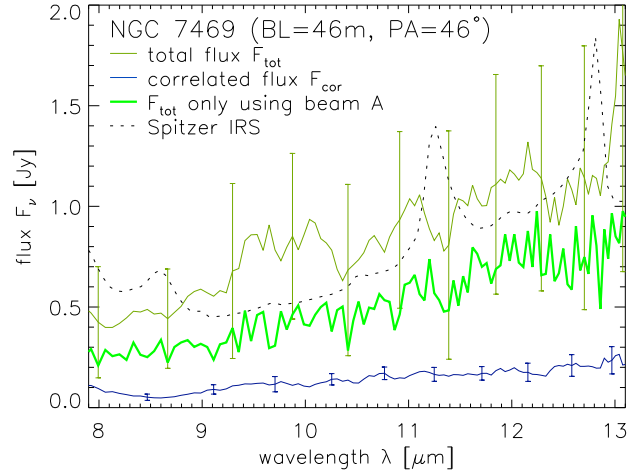
Fig. 6. Results of the MIDI measurements for IC 4329A. The correlated flux spectrum (blue) and the total flux spectrum (green) are compared to the TIMMI2 spectrum from Siebenmorgen et al. (2004, dotted line). For the sake of clarity, the errors of the MIDI data are only indicated every tenth wavelength bin.

Fig. 7. Correlated (blue) and total (green) flux spectra of NGC 7469. For comparison, the flux measured by Spitzer is traced by the dotted line (cf. also Fig. 6 in Weedman et al. 2005). The total flux, only determined using beam A (UT3), is plotted in dark green. For the sake of clarity, error bars are only given every tenth wavelength bin.

ular baseline orientations ($PA \sim 31°$ and $PA \sim 128°$). Changes in the correlated flux could thus be interpreted as an indication for an elongated morphology. On the other hand, variability of up to ~60 % has been observed in the mid-infrared at $10.6 \mu m$ (Neugebauer & Matthews 1999) for 3C 273, so that the variations could have been caused by intrinsic changes in the spectrum of the quasar. All Spitzer spectra (the two Spitzer spectra shown in Fig. 5 from 2007 Feb 28 and 2007 Jun 28 as well as the spectrum in Hao et al. 2005 from 2004 Jan 06) show variations of less than 10 % and are also consistent with the VISIR and TIMMI2 photometries. Hence we see no evidence for any significant variability during our observations. This is also supported by submm data of the source obtained as part of the monitoring program initiated by the SMA (Gurwell et al. 2007): 3C 273 appeared in a relatively quiescent state in February 2007 and April 2008. This leads to the conclusion that we mainly measured the emission from warm dust which is not expected to change on shorter timescales and that the change in the correlated flux is more likely to be caused by an elongated morphology. A more detailed analysis of the MIDI data for 3C 273 will be given in Jaffe et al. in preparation.

4.6. IC 4329A

IC 4329A is an edge-on spiral galaxy at a distance of 65 Mpc ($4793 \pm 27 \, \mathrm{km \, s^{-1}}$, 1 arcsec = 320 pc, de Vaucouleurs et al. 1991) hosting a Seyfert 1.2 nucleus. The nuclear activity might be triggered by the proximity to IC 4329, a giant elliptical galaxy. As one of the brightest X-ray sources, it has been mainly studied in this wavelength range.

Fig. 6 shows the results of the MIDI measurements as well as the spectrum obtained with TIMMI2 from Siebenmorgen et al. (2004). While the MIDI correlated flux spectrum seems to be well determined, the total flux spectrum has large uncertainties, mainly because the measured fluxes for the two telescopes differ by more than a factor of 2 (cf. Appendix A.7). The total flux spectrum measured by MIDI lies between the slightly lower TIMMI2 spectrum and the slightly higher spectra obtained with

larger apertures, e.g. the Spitzer IRS spectrum (not shown here) or the spectrum presented in Roche et al. (1991). As the total flux measurement with MIDI is consistent with these other spectra, we assume the total flux of the source to rise from ~0.5 Jy at $8 \mu m$ to 1.1 Jy at $13 \mu m$ for the following. The correlated flux is slightly lower but nevertheless consistent with these values considering the uncertainties. The conclusion is that the nucleus of IC 4329A is essentially unresolved. This means that the bulk of the mid-infrared emission is concentrated on scales smaller than the spatial frequency corresponding to the baseline length for our measurement ($BL = 46.6$ m), that is, on scales roughly smaller than 30 mas, which corresponds to ~10 pc in IC 4329A.

4.7. NGC 7469

NGC 7469 is a well-studied, barred spiral galaxy at a distance of about 65 Mpc ($v_{hel} = 4843 \pm 5 \, \mathrm{km \, s^{-1}}$, Beswick et al. 2002; 1 arcsec = 320 pc), which hosts a classical Seyfert 1 nucleus. It is also classified as a Luminous InfraRed Galaxy (LIRG) and it harbours a face-on circumnuclear starforming ring with a size of 1.0 kpc (3 arcsec), which has been detected at radio, optical and infrared wavelengths (Díaz-Santos et al. 2007, and references therein). High resolution studies in the mid-infrared have been carried out by Miles et al. (1994); Soifer et al. (2003); Gorjian et al. (2004) and Galliano et al. (2005). They have found that 50 to 60 % of the total mid-infrared emission in the centre of this galaxy (i.e. within ~6 arcsec = 2 kpc) originate from the star forming ring, while only the remaining 40 % to 50 % (~0.5 Jy) can be ascribed to the compact nuclear source. Using deconvolved images obtained with the Keck telescope, Soifer et al. (2003) marginally resolve the nuclear source. They report a structure of (<0.04) × 0.08 arcsec (13 × 26 pc) with a position angle of 135°.

The results of the first MIDI observing run are shown in Fig. 7. These, however, need to be discussed: we find a significant difference between the pipeline reduced total flux spectrum (thin green line) and the one obtained only from beam A (UT3, see Appendix A.9; thick green line). Which one is credi-

ble? The best mid-infrared spectrum available for comparison is from Spitzer. To a large degree, it contains the flux from the star forming ring, as can be deduced from the prominent PAH features and emission lines. It is therefore an extremely conservative upper limit for the MIDI data and the expectation from the mid-infrared imaging is that the total flux measured by MIDI should be roughly half of that of Spitzer. As the pipeline reduced spectrum lies above that of Spitzer for most of the N band, we consider this determination to be erroneous. On the other hand, the total flux spectrum only determined using beam A is on levels of roughly 50 to 80 % of the continuum component in the Spitzer spectrum and it is consistent with the photometric values published for the nuclear component in Soifer et al. (2003); Galliano et al. (2005) and Raban et al. (2008): 0.65 Jy at $12.5\,\mu m$, 0.56 Jy at $11.9\,\mu m$ and 0.67 Jy at $11.9\,\mu m$ respectively. Therefore we consider the total flux only using the A photometry as the best estimate for the total flux spectrum, F_{tot}.

From Fig. 7 it appears that the correlated flux spectrum, with $F_{cor} \sim 0.1-0.2$ Jy, is significantly lower than the total flux spectrum, i.e. $F_{cor} < F_{tot}$. Our interferometric observations were obtained with a position angle of $PA = 45°$, which is more or less along the minor axis of the extended structure from Soifer et al. (2003). The fringe spacing of the interferometer with a baseline length of $BL = 46$ m is on the order of 25 mas (=8 pc in NGC 7469). Due to the large errors in our data and especially the large uncertainty in the total flux spectrum, the determination of a size estimate is very ambitious. But considering that fringes could be tracked and that the correlated flux seems to be significantly lower than the total flux, the overall size of the source cannot be much different from the fringe spacing. Hence, we estimate the size of the dust distribution to be on the order of 10 pc. Note that, for the measurement on the second baseline with $BL = 51$ m and $PA = 107°$, the correlated flux seems to have been even lower, because no fringes could be tracked (see Appendix A.9). This could be an indication that the source is slightly more resolved in this direction. This would be in rough agreement with the extended structure described by Soifer et al. (2003). More data with a higher signal to noise ratio will be needed to confirm this speculation.

5. Summary of the observations and their implications

In the MIDI AGN snapshot survey, interferometric observations in the mid-infrared were attempted for a set of ten AGN. Out of these ten sources, an interferometric signal could be detected for eight sources and only for two no measurement with MIDI was possible at all. For the latter two sources (NGC 3281 and NGC 5506, see Appendices A.4 and A.8), no stable AO correction could be obtained with MACAO using the optical nuclei of these two galaxies. Hence, the observation failed during the acquisition process and not because an interferometric signal could not be detected by MIDI. For all of the eight sources where a stable AO correction could be achieved at some point, an interferometric signal was detected. This means that the true detection rate of a fringe signal by MIDI itself for the AGN in the snapshot survey is 100 %. For all except one of these eight sources, fringes could also be tracked, that is, the zero OPD position could be continuously determined. Only for IRAS 05189-2524, the online tracking software was not able to determine the zero OPD position. This was only possible in post-processing (see Appendix A.2). For six of the seven remaining sources, the faintness and extent of the nuclei in the optical were still challenging for MACAO. Mainly the photometric observations were

affected by having to use the AO systems at their limits: in many cases a stable AO correction was not possible while chopping. The chopping constitutes an additional complication for the AO system, since in every chopping cycle the AO loop has to be opened for the off target position (sky position) and then closed again for the on target position. On the other hand, for the interferometric measurement no chopping is needed and generally a more stable AO correction is achieved (see Sect. 3). Only for MCG-05-23-016 were there no AO problems at all. In fact, this is the only galaxy from the snapshot survey, where the AO correction was performed using a separate Coudé guide star. For all other galaxies, the more or less extended and obscured nuclei were used.

The overall perfomance of the adaptive optics systems depends on several factors, the most important being (1) the performance of the individual adaptive optics units, (2) the brightness and spatial extent of the object used for guiding and (3) the atmospheric conditions. For (1) we note that, during our observations, the MACAO unit on UT2 caused the bulk of the problems. In general, this unit produced a worse wavefront correction – resulting in a reduced PSF quality – than the other units and it was often this unit which failed totally to close the loop. A more robust correction is achieved using bright and pointlike Coudé guiding sources. To date, for all except one of the faint sources observations have been tried with Coudé guiding on the nucleus, although for some of the sources a possible guide star is in range (see Table 2). Especially in the case of NGC 7469, and maybe also for NGC 3281, future observations should be tried using the guide star available. Finally, the probability of a stable AO correction depends sensitively on the atmospheric conditions at the time of observation: good seeing conditions and long coherence times increase the chances of a stable AO correction and hence are necessary for the interferometric observation of faint AGN with the VLTI.

From the high detection rate of fringes in the snapshot survey, we deduce that the ultimate limit for the detection of an interferometric signal with MIDI has not yet been reached. From our data on IRAS 05189-2524, we infer that the limit for the detection and tracking of fringes with MIDI is on the order of 0.1 to 0.2 Jy. This limit is however only reached when an optimised mask and optimised data reduction settings are applied. At the moment, this can only be done in post processing. For the current implementation of the software at the VLTI, the limit is approximately a factor of 2 higher, on the order of 0.3 Jy. Simply using longer integration times and redundant measurements will not improve the detectability of even weaker sources, as it will not be possible to continuously determine the zero OPD position in real time. An external fringe tracker will be necessary, if even fainter sources are to be observed. Furthermore, we note that the detection and the recording of the interferometric signal is normally not the only goal of a MIDI observation. Instead, full data sets consisting of both the interferometric signal as well as the photometry are required to scientifically evaluate the data. This is especially the case if only a few visibility points are observed (as is the case for the sources presented here) and if a direct comparison between several measurements of the correlated flux at different baseline lengths and orientations is not possible. Even if a stable AO correction is achieved, the main limitations are still connected with the robust determination of the total flux spectrum from the photometry: it is the total fluxes that show large (statistical) errors due to the constant variability of the background in the mid-infrared. Even for stable atmospheric conditions, total fluxes on the order of 1.0 Jy have a statistical error of up to 20 %. Less stable atmospheric conditions

Table 3. Characteristics derived from the interferometric observations of the AGN in the snapshot survey (marked by asterisks) and other AGN studied by MIDI.

Galaxy name (1)	type (2)	D [Mpc] (3)	BL [m] (4)	$F_{tot,12\mu m}$ [Jy] (5)	$F_{cor,12\mu m}$ [Jy] (6)	$s_{12\mu m}$ [pc] (7)
NGC 1068	Sy 2	14	33.6	16.50	4.00	3.2
NGC 1068	Sy 2	14	79.9	16.50	1.20	>1.8
* NGC 1365	Sy 1.8	18	46.6	0.51	0.28	2.0
* NGC 1365	Sy 1.8	18	54.4	0.34	0.25	<2.7
* NGC 1365	Sy 1.8	18	62.3	0.47	0.32	1.1
* MCG-05-23-016	Sy 2	35	46.1	0.60	0.35	2.8
* Mrk 1239	Sy 1.5	80	43.0	0.57	0.48	<7.0
NGC 3783	Sy 1	40	68.6	1.25	0.50	3.6
NGC 3783	Sy 1	40	64.9	1.02	0.54	3.1
* NGC 4151	Sy 1.5	14	35.8	1.21	0.27	>2.6
* 3C 273	QSO	650	36.7	0.32	0.32	<67.
* 3C 273	QSO	650	29.7	0.29	0.20	<108.
* IC 4329A	Sy 1.2	65	46.6	1.00	0.75	<10.8
Circinus	Sy 2	4	20.7	10.20	1.80	>1.5
Circinus	Sy 2	4	62.4	10.20	1.10	>0.6
* NGC 7469	Sy 1.2	65	46.4	0.70	0.17	10.5

Notes: The columns are (1) the name, (2) the type and (3) the distance of the galaxy (all repeated from Tab. 1); (4) the baseline length for the respective observation; (5) the total and (6) correlated fluxes at $12\,\mu m$ as well as (7) the approximate size of the emitter at $12\,\mu m$.

immediately lead to larger statistical errors, as can be directly deduced from the MIDI observations of Centaurus A (see Fig. 1 in Meisenheimer et al. 2007). Due to these limitations, for very faint sources, it may be better to skip the photometric measurements and use relative changes among the correlated fluxes to characterise the emitter. This is, in fact, how observations are commonly carried out with radio interferometry.

In general, the MIDI data nevertheless appear to be reasonable and trustworthy. Especially the good agreement between the MIDI measurements and the mid-infrared data used for comparison in the case of MCG-05-23-016 and Mrk 1239 is reassuring. It shows that MIDI produces reliable results even at its sensitivity limit when the observational strategy is adapted accordingly and when complete data sets are obtained. For faint sources, it is imperative to carry out MIDI observations with significantly increased exposure times (e.g. NDIT = 8000 instead of NDIT = 2000 for the photometry) and a certain degree of redundancy (e.g. by repeating the error-prone photometric observations) in order to reach an acceptable signal-to-noise ratio. This and the often longer acquisition procedure lead to a considerably larger amount of time, up to 1 h, needed for the measurement of the science target alone. Together with the calibrator observations, a full, calibrated visibility point for a faint source thus requires up to 1.5 h of observing time.

6. Discussion

Together with the other AGN observed with MIDI, the data presented here make up the spectra with the highest spatial resolution of cores of AGN in the mid-infrared. They allow us to directly analyse the properties of the circumnuclear dust which is heated by the central engine of the AGN.

In the following, two aspects of the sources will be discussed in greater detail, namely the properties of their spectra (Sect. 6.1) and the size of their emission region (Sect. 6.2). The size estimates used in the following discussion are those derived

in Sect. 4, taken at a wavelength of $12\,\mu m$. For those galaxies where plots of the wavelength dependency of the size are given, i.e. for NGC 1365, MGC-05-23-016 and Mrk 1239, the values are marked by filled circles in the respective figures (Figs. 2 and 3).

The values of the sizes at $12\,\mu m$ are listed in Table 3 for every visibility point together with the galaxy type, the distance of the galaxy and the baseline length of the MIDI observation. Also listed are the correlated and the total flux values at $12\,\mu m$, $F_{cor,12\mu m}$ and $F_{tot,12\mu m}$. For $\lambda = 12\,\mu m$, the MIDI measurements have the highest signal to noise ratio and they are least affected by the edges of the N band or the atmospheric ozone absorption feature.

The values for the sources of the snapshot survey were complemented by values for selected visibility points of other Seyfert galaxies, for which MIDI results have been published, that is, for NGC 1068 (Raban et al. 2009), for the Circinus galaxy (Tristram et al. 2007) and for NGC 3783 (Beckert et al. 2008). The sizes for these additional sources were determined in the same way as for the sources of the snapshot survey. Due to its nature as a radio galaxy with a strong non-thermal component in the mid-infrared, Centaurus A was not included in the current analysis.

6.1. Spectral features

The most characteristic feature of AGN in the N band is their absorption or emission by silicate dust, which leads to a broad absorption trough or emission bump covering almost the entire wavelength range between 8 and $13\,\mu m$. For typical geometries of AGN tori, the feature is expected to appear in absorption for type 2 objects and in emission for type 1 objects. Indeed, for most AGN, including the sources of the snapshot survey, a silicate absorption or emission feature is present in high signal to noise Spitzer spectra, even if the signature is very weak (see e.g. Hao et al. 2005; Weedman et al. 2005; Buchanan et al. 2006). The MIDI spectra presented here only show indications for silicate absorption or emission for three sources of the snapshot survey: MCG-05-23-016 (feature in absorption, Seyfert 2 galaxy), Mrk 1239 (feature in emission, Seyfert 1.5 galaxy) and 3C 273 (also in emission, type 1 quasar). The feature is relatively weak in all of these three sources, especially in comparison to the deep absorption features found in the two brighter Seyfert galaxies studied by MIDI, NGC 1068 and the Circinus galaxy (both Seyfert 2 galaxies; Tristram et al. 2007; Jaffe et al. 2004; Raban et al. 2009). In fact, it is surprising that the two brightest AGN in the mid-infrared also show the strongest absorption feature. For the Circinus galaxy and even more so for NGC 1068, changes in the silicate absorption depth have been observed between the total flux spectra and the correlated flux spectra. For the sources of the snapshot survey however, we find no significant difference in the feature strength between the single dish measurements (or the spectra used for comparison) and the interferometric measurements. While we can thus rule out any dramatic changes in the strength of the feature for the sizes probed by our interferometric measurements, any small changes may be hidden by the low signal to noise ratio of the data compared to that of the two bright sources. It is interesting to note that, for the two type 1 AGN, Mrk 1239 and 3C 273, the peak of the emission feature is located at $11\,\mu m$. The peak is thus offset against the maximum at $9.7\,\mu m$ of the absorption coefficient of interstellar dust, which is dominated by amorphous Olivine ($[Mg, Fe]_2SiO_4$, Kemper et al. 2004). The shift of the position of the silicate feature is best explained by more aluminum-rich
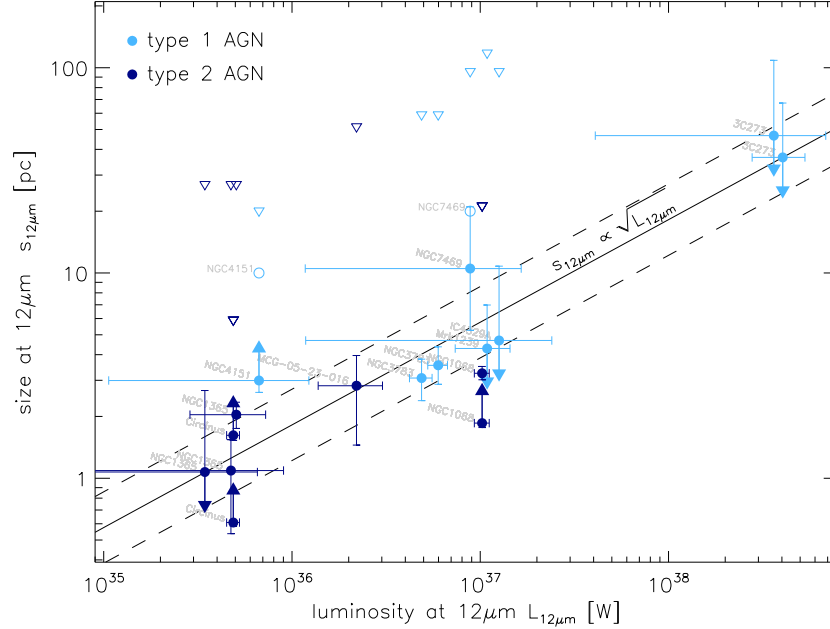
Fig. 8. Size of the mid-infrared emitter as a function of its monochromatic luminosity in the mid-infrared for the AGN studied with MIDI (filled circles with error bars). Upper and lower limits on the size estimates are marked by arrows. The fitted size–luminosity relation for $p = 1.8 \cdot 10^{-18}$ pc $\cdot$ (W)$^{-0.5}$ is traced by the black line. The scatter of the measurements around this relation is 0.6 dex (black dashed lines). The physical scales in the respective galaxies corresponding to an angular resolution of 0.3 arcsec (diffraction limit of an 8 m class telescope at 12 μm) are labelled by open triangles. The size of the resolved emission in NGC 4151 (10 pc) from Neugebauer et al. (1990) and in NGC 7469 (~20 pc) from Soifer et al. (2003) are shown by open circles.

silica such as Augite (Ca$_2$Al$_2$SiO$_7$), which has a higher dissociation temperature and which also seems to be responsible for the changes in the absorption profile observed for NGC 1068 (Jaffe et al. 2004; Raban et al. 2009).

Finally, we note that there are no signs of the PAH features or the line emission, which are seen in the spectra used for comparison (especially for NGC 7469, see Fig. 7), in either the correlated flux spectra or in the total flux spectra. The PAH features are associated with star formation and are destroyed by the hard UV radiation in the vicinity of the AGN. Their absence thus indicates that the regions we are probing are dominated by the radiation field of the AGN.

6.2. Sizes of the dust distributions

For simple geometries, the visibility reaches a first minimum when the fringe spacing $\Lambda = \lambda/BL$ (i.e. the "resolution") of the interferometer equals the characteristic size of the source. Therefore, the *FWHM* of a Gaussian distribution is a good estimate for the spatial scales over which the bulk of the emission is distributed, as long as $0.2 \lesssim V \lesssim 0.8$. For $V \lesssim 0.2$, most of the flux has been resolved out while for $V \gtrsim 0.8$ the bulk of the emission remains unresolved. Only lower or upper limits on the sizes can be given in these cases.

One has to be careful not to overinterpret the size values derived from the interferometric measurements. As shown by models of AGN tori (e.g. Hönig et al. 2006; Schartmann et al. 2008) or revealed by our detailed studies of the Circinus galaxy and of NGC 1068 (Tristram et al. 2007; Raban et al. 2009), the nuclear mid-infrared emission of AGN is complex, with structures on a variety of size scales. An interferometric detection with MIDI merely indicates that the correlated flux that was measured is contained in a relatively compact region with a size not much more than Λ. The size scales sampled by the single dishes used to derive the total flux spectra are much larger than those probed by the interferometer. It is not clear from only one (or very few) visibility measurements, how the flux is actually distributed between the two characteristic size scales and it is very unlikely that the real brightness distribution follows a Gaussian dependency. This is especially the case for type 1 AGN, where the infrared flux is possibly also affected by the flux from the accretion disk, which appears as a point source. The limits derived from the MIDI data for type 1 AGN are hence not only a measure for the size of the dust emission alone, but for the combination of the flux of the torus and of the accretion disk. Because the point source adds a constant to the visibility, independent of the spatial frequency (i.e. also the baseline length), further measurements (with the same position angle but different baseline lengths) must be obtained in order to disentangle the individual components.

For NGC 1068 and the Circinus galaxy, our simple method to estimate the size assuming a Gaussian brightness distribution can be verified in comparison to fitting a model of the emitter to several interferometric measurements. In the present analysis, the measurements with the shortest and longest available baselines for these two galaxies were included. The sizes determined by our simple method (see Table 3) lie between the sizes of the two components of the models in Raban et al. (2009) and Tristram et al. (2007): 1.5 to 4.0 pc for NGC 1068 and 0.4 to 2.0 pc for the Circinus galaxy. We thus conclude that our size estimates are indeed realistic.

In Fig. 8, the sizes of the emission regions are compared to the monochromatic luminosity at 12 μm, which is given by $L_{12\,\mu m} = 4\pi D^2 \nu F_{\text{tot},12\,\mu m}$ with $\nu = 2.5 \cdot 10^{13}$ Hz. Studying the

sizes as a function of $L_{12\,\mu m}$ instead of $F_{tot,12\,\mu m}$ breaks any dependency of the size on the distance D, except for selection effects (more distant objects being more luminous). The physical scales corresponding to an angular resolution of 0.3 arcsec, which is the diffraction limit of an 8 m class telescope at $12\,\mu m$, are also shown for each galaxy (open triangles). As the mid-infrared cores of all AGN are essentially unresolved by single dish observations, these size scales are strict upper limits for the sizes of the dust distributions.

For similar geometries and volume filling factors, the size of the torus at a certain wavelength, s_λ, should be a function of its monochromatic luminosity, L_λ, at this wavelength: $s_\lambda = p_\lambda \cdot (L_\lambda)^{0.5}$ or $\log(s_\lambda/\mathrm{pc}) = q_\lambda + 0.5 \cdot \log(L_\lambda/\mathrm{W})$, where p_λ and q_λ are constants largely depending on the volume filling factor and/or the optical depth of the torus. The relation reflects that an object of twice the size has four times more emitting surface. Indeed most of our measurements agree with the above relation and for $\lambda = 12\,\mu m$ we find $p_{12\,\mu m} = (1.8 \pm 0.3) \cdot 10^{-18}\,\mathrm{pc}\cdot(\mathrm{W})^{-0.5}$ and $q_{12\,\mu m} = -17.7 \mp 0.2$, respectively. The scatter of the individual sources around the relation is 0.6 dex (see Fig. 8). It can be largely explained by the uncertainties in our measurements. However, also differences in the actual geometry and orientation as well as in the filling factor of the dust distribution have a significant impact on the apparent size of the emission region. For an optically thick blackbody emitter with the size s, the luminosity is given as $L_\lambda = \pi s^2 \nu F_{bb}(\nu, T)$. This can be rearranged to $s = (\pi \nu F_{bb}(\nu, T))^{-0.5} \cdot (L_\lambda)^{0.5}$. For $p_\lambda = (\pi \nu F_{bb}(\nu, T))^{-0.5}$ this is identical to the above relation. For a temperature of $T = 300\,K$, taken as an average value for the temperatures suggested by the slopes of the spectra, we obtain $p_{12\,\mu m} \sim 1.8 \cdot 10^{-18}\,\mathrm{pc} \cdot (\mathrm{W})^{-0.5}$. This implies that the mid-infrared emission is consistent with originating in a more or less optically thick and thus compact dust distribution with an average temperature of $300\,K$.

At the first glance, there seems to be a tendency for type 1 objects to have more extended dust distributions than type 2 objects: while the nuclear dust distribution in NGC 1068 appears relatively compact in comparison to all other galaxies, the warm dust in NGC 4151 and NGC 7469 seems to be more extended than average. Further evidence in this direction comes from Neugebauer et al. (1990) and Soifer et al. (2003), who partially resolved the mid-infrared cores in just these two galaxies. Their size estimates, 10 pc for NGC 4151 and $(<13) \times 26$ pc for NGC 7469, are also shown in Fig. 8 (open circles; averaged to ∼20 pc in the case of NGC 7469) and suggest even more extended emission regions than measured by our interferometric measurements. In the case of NGC 7469, the apparently larger extent may partially be explained by a contamination with the extended emission from the surrounding starburst to the single dish spectra, although this contamination cannot be very large due to the lack of PAH signatures in our total flux spectrum. In the case of NGC 4151, however, there is no circumnuclear starburst contribution that could contaminate the single dish measurements. It seems that the warm dust in this galaxy is more extended for its luminosity than that of any other galaxy of our sample. This is probably caused by the emission from dust in the ionisation cones, which is extended on the scales of 3.5 arcsec = 230 pc (Radomski et al. 2003). Thus, it appears that a major fraction of the mid-infrared emission in this source actually originates in the ionisation cones and not in the torus itself. Together with the relatively red spectrum at the centre, it seems that this galaxy is also a special case according to the standard picture in which most of the mid-infrared emission is expected to originate in the dusty torus. A more detailed analysis of the

interferometric data, including new observations, will be necessary to substantiate this finding.

Apart from these indications for individual outliers to the size-luminosity relation, there is no indication from our data that the size of the emission region differs significantly between type 1 and type 2 objects. That means that the sizes of the distributions of warm dust are of the same order in both types of nuclei. This is in strong support of the unified picture, where the dust distributions in both AGN types are assumed to be the same. This finding also agrees well with recent radiative transfer calculations of clumpy AGN tori, where the appearance of the tori is relatively similar in the mid-infrared (Schartmann et al. 2008, 2009).

6.3. Elongation of the dust emission

We have tentatively detected an elongated mid-infrared emission region for three sources: NGC 1365, 3C 273 and NGC 7469. In the latter case, the elongation has been previously detected by Soifer et al. (2003). For NGC 1365, the elongation derived from our measurements is roughly oriented perpendicularly to the axis of symmetry of the system, which is defined by the axis of the radio jet or the ionisation cone.

This is, again, in agreement with the expectation in the standard unified paradigm of AGN and to the results found for the three brighter AGN (NGC 1068, the Circinus galaxy and Centaurus A), where dust disks roughly perpendicular to the axis of symmetry of the systems were found (Raban et al. 2009; Tristram et al. 2007; Meisenheimer et al. 2007). More measurements are, however, needed to confirm these results.

7. Conclusions

In the MIDI AGN snapshot survey, high resolution interferometric observations of ten active galactic nuclei were attempted in the mid-infrared with MIDI at the VLTI. The goal was to determine, which further AGN, in addition to the previously investigated sources NGC 1068, the Circinus galaxy and Centaurus A, are suitable for studies with MIDI and to derive first estimates for the sizes of the emission regions in the mid-infrared.

The observations were performed at the sensitivity limit of MIDI and of the VLTI. We find that, currently, the main limitation for the observations is the ability to obtain a stable AO correction and to obtain a secure total flux (i.e. single dish) measurement. No interferometric measurements could be carried out for two of the sources targeted, because the nuclei of these galaxies were too faint and too extended for the MACAO systems to provide an adaptive optics correction.

For the remaining eight sources, an interferometric signal could indeed be detected and for seven of them the signal was strong enough to derive correlated flux spectra. Together with the three brighter targets NGC 1068, the Circinus galaxy and Centaurus A as well as with two further AGN, NGC 3783 (Beckert et al. 2008) and NGC 424 (Hönig et al. in preparation b), this gives a total number of 12 extragalactic sources for which fringes could be tracked with MIDI. All of these objects are worth further investigations and more detailed observations are underway.

The silicate feature at $10\,\mu m$ is detected in the MIDI data for only 3 of the 10 sources. For these three sources, it provides evidence for some difference between type 1 and type 2 AGN as expected in the unified model: the feature appears in emission for one type 1 object and in absorption for two type 2 objects.

For the sources where size estimates for the emission regions could be determined, we have found that the emission regions have sizes between 1 and 10 pc roughly scaling with $\sqrt{L_{MIR}}$ and for more or less optically thick emission. This "size-luminosity relation" is consistent with the emission originating in compact and warm ($T \sim 300\,\text{K}$) dust distributions, which are heated by the central engines of the AGN. In the spectral features as well as in their sizes have we found no significant differences between type 1 and type 2 AGN, indicating that the types of objects have similar signatures of their dust distributions in the mid-infrared.

Larger differences in size appear between individual objects and we have found that the individual members of a class differ from each other more than suggested by the standard picture of the dusty torus. This is in agreement with recent hydrodynamical models of AGN tori which show that the mid-infrared properties significantly depend on the detailed configuration of the non-smooth dust distribution.

Appendix A: Remarks on the observations and the data reduction for the individual sources

In the following, the observations and the data reduction for the individual sources of the snapshot survey are presented in greater detail. The observation log is given in Table A.1.

A.1. NGC 1365

This source was successfully observed several times during the observation runs on 2006 Sep 11 and on 2007 Nov 24, using the UT2 – UT3 and the UT3 – UT4 baselines, respectively.

During the first run, the ambient conditions were fair, with a seeing of 1.1 to 1.4 arcsec. Although the MACAO unit on UT2 was unable to securely lock on the extended nucleus under these conditions, a fringe signal could be detected and tracked (sci12, see Table A.1). While the quality of the subsequent photometry of beam A is relatively good, no signal is present in the photometry of beam B: no stable AO correction could be achieved while chopping on UT2. For this reason, the photometry was replaced by a portion of the A photometry with little background variations in order to be able to reduce the data using the standard data reduction routines. Additionally to the standard reduction routine, which relies on both photometries and yields an "averaged two-dish total spectrum" of the source, we determined the total flux using only the photometry of beam A for both NGC 1365 and the associated calibrator HD 026 967 (cal12). The information of beam B was disregarded completely. As for the standard data reduction, the calibration was carried out using the template spectrum of the star from the database by Roy van Boekel (private comm.). We find that the two determinations of the total flux spectrum are consistent with each other within a fraction of their errors.

Two further attempts (sci13 and sci14) to track the fringes of this source on 2007 Nov 24 failed; no stable tracking could be achieved.

More successful observations of the source were carried out during the second run, although the ambient conditions were comparable to those on 2006 Sep 11. A total of 4 successful fringe tracks and two sets of photometric data could be obtained. However, the data reduction was again not straight forward due to problems with the photometry of the first data set (sci33): the background in the photometry of beam A (UT4) was extremely unstable, so that only a subset of the frames, where the background is relatively stable, were selected for the data reduction. The last three fringe tracks (sci35, sci36 and sci37) were observed consecutively without reacquisition of the source and the length and orientation of the baseline only changed insignificantly. Therefore, the three measurements were almost identical and they were averaged to give one visibility point.

A.2. IRAS 05189-2524

For IRAS 05189-2524 (LEDA 17155), a Seyfert 2 galaxy located at a distance of 170 Mpc ($12\,760 \pm 54\,\text{km\,s}^{-1}$, Huchra et al. 1983; 1 arcsec = 850 pc), two observation attempts were carried out. Although the acquisition succeeded with UT3 on 2006 Sep 11, it completely failed for UT2. Hence, no data were obtained on this occasion. Only during the second attempt on 2007 Nov 24 with the UT3 – UT4 baseline, a stable AO correction with MACAO was achieved. A very weak signal is present in the fringe search, although this was only noticed in post processing using the optimised mask and the parameter settings described in Sect. 3. The fringe track, which was observed "blind", i.e. without knowing the exact position of zero OPD at the time of the observation, also shows a very faint signal, while the OPD drifted over the zero OPD position. However, the signal was too weak for the observing software to stabilise the OPD and hence not enough frames were recorded to allow a confident determination of the correlated flux. From the acquisition images it seems that the two beams were misaligned by more than 2 pixels (=0.17 arcsec), which is slightly more than $HWHM$ = 0.15 arcsec, the half width half maximum of the PSF averaged over the N band. This means that the beam overlap was such that only 75 % of the flux were able to interfere. From the few frames where an interferometric signal is present, we estimate that the correlated flux rises from ~0.1 Jy at 8 μm to ~0.2 Jy at 13 μm. Taking into account the correction for the beam overlap, the correlated flux in IRAS 05189-2524 seems to have been on the order of 0.1 to 0.3 Jy. This is significantly less than the total flux spectrum measured by Siebenmorgen et al. (2004), which rises from 0.3 to 1.0 Jy from the short to the long wavelength end of the N band, potentially indicating that the source is resolved. Unfortunately, no photometry confirming this conclusion was observed for IRAS 05189-2524 with MIDI. This case shows how important it is to also obtain photometric information even for those sources where no fringes could be detected or tracked. Then a lower limit for the size of the emitter could be derived.

A.3. MCG-05-23-016 and Mrk 1239

One full visibility measurement for MCG-05-23-016 and two full measurements for Mrk 1239 were obtained on 2005 Dec 19. Double photometric measurements of 8000 frames each for every visibility point were carried out in order to increase the signal-to-noise and to obtain redundant measurements in case of problems. Indeed, for the second observation of Mrk 1239 (sci03, see Table A.1), the MACAO loop was open for a portion of the second photometry of beam B (UT2). The faulty photometry was replaced by the corresponding one taken during the first observation (sci02, see Table A.1).

Table A.1. Observation log for the AGN of the snapshot survey, including the detector integration times (DIT), the number of frames (NDIT) for the fringe tracks and photometries as well as the lengths (BL) and position angles (PA) of the projected baselines. The times, ambient values and baseline properties relate to the start of the fringe track.

Date and time [UTC]	Object		DIT [s]	NDIT fringes	phot.	Airmass	Seeing[a] ['']	BL [m]	PA [°]	Associated calibrator and comments
2005 Dec 19:	**UT2 – UT3**		**076.B-0038(A)**							
05:07:40	HD 090 610	cal01	0.018	8000	2500	1.72	0.91	45.1	0.9	ok
06:39:51	MCG-05-23-016	sci01	0.018	12000	2 × 8000	1.12	0.75	46.1	24.3	cal01 ok
07:31:59	Mrk 1239	sci02	0.018	12000	2 × 8000	1.14	0.70	41.1	36.3	cal02 ok
08:15:17	HD 083 618	cal02	0.018	8000	2500	1.09	0.51	43.9	41.7	ok
08:47:23	Mrk 1239	sci03	0.018	12000	2 × 8000	1.09	0.55	44.8	42.9	cal03 second part of photometry B contains no signal
09:27:55	HD 083 618	cal03	0.018	8000		1.13	1.00	46.3	45.3	replaced missing photometry by that of cal02
2006 Sep 11:	**UT2 – UT3**		**077.B-0026(B)**							
05:00:21	HD 220 009	cal11	0.018	8000	4000	1.16	1.15	44.1	45.0	ok
06:09:20	NGC 7469	sci11	0.018	8000	8000	1.35	1.12	46.4	46.3	cal11 photometry B contains no signal (AO problem on UT2)
07:00:40	HD 026 967	cal12	0.018	8000	4000	1.24	1.48	46.6	17.9	bumpy fringe track
07:42:55	NGC 1365	sci12	0.018	8000	8000	1.06	1.31	46.6	31.1	cal14 photometry B contains no signal (AO problem on UT2)
08:28:27	HD 026 967	cal13	0.018	8000		1.08	1.32	46.4	32.1	replaced missing photometry by that of cal12
08:44:20	HD 036 597	cal14	0.018	8000	4000	1.15	1.27	46.4	22.5	ok
09:36:20	NGC 1365	sci13	0.018	8000		1.03	1.37	45.1	45.7	no fringe track, no photometry
09:41:27	NGC 1365	sci14	0.018	8000		1.04		44.9	46.3	no fringe track (but weak signal), no photometry
2007 Feb 07:	**UT2 – UT3**		**078.B-0031(A)**							
03:36:01	HD 081 420	cal21	0.018	8000	4000	1.13	0.65	41.4	33.5	no offset tracking mode, phot B bad!
05:41:06	3C 273	sci21	0.018	8000		1.37	0.69	35.2	27.0	no fringe track (started at wrong OPD position)
05:50:44	3C 273	sci22	0.018	8000		1.33	0.83	35.8	28.7	lost fringe track, no photometry
06:04:10	3C 273	sci23	0.018	8000		1.29	0.74	36.7	31.0	cal22 no photometry
06:08:32	3C 273	sci24	0.018	8000		1.27	0.71	37.0	31.6	cal22 no photometry
06:31:50	HD 098 430	cal22	0.018	8000	4000	1.02	0.60	45.9	38.6	ok
07:49:59	NGC 4151	sci25	0.018	8000		2.27	0.67	34.6	61.9	no fringe track (but weak signal), no photometry
08:03:42	NGC 4151	sci26	0.018	8000	4000 (A)	2.29	0.49	35.8	60.8	cal22 lost fringe track, only A photometry observed
08:43:55	IC 4329A	sci27	0.018	8000		1.02	0.62	46.6	35.7	cal23 no photometry
08:49:02	IC 4329A	sci28	0.018	8000	4000	1.01	0.69	46.6	36.3	cal23 photometry observed after cal23
09:08:18	HD 123 123	cal23	0.018	8000	4000	1.01	0.56	46.6	36.6	ok
2007 Nov 24:	**UT3 – UT4**		**080.B-0258(A)**							
00:00:39	HD 220 009	cal31	0.018	8000	4000	1.16	1.15	60.9	108.1	ok
01:07:41	NGC 7469	sci31	0.018	8000		1.32	1.08	51.9	106.8	cal31 no fringe track (but weak signal), IRIS problems on UT3
01:12:56	NGC 7469	sci32	0.018	8000		1.34	1.17	51.1	106.9	cal31 lost fringe track, IRIS problems on UT3, no photometry
01:53:47	NGC 1365	sci33	0.018	8000	8000	1.15	1.37	54.4	92.8	cal32 problems with IRIS
02:38:26	HD 016 815	cal32	0.018	8000	2500	1.04	1.46	61.3	105.5	ok
03:10:23	IRAS 05189-2524	sci34	0.018	8000		1.23		51.1	96.0	cal32 lost track, problems with IRIS, no photometry
03:33:48	HD 016 815	cal33	0.018	8000		1.04	1.11	62.5	114.0	no photometry
03:51:36	NGC 1365	sci35	0.018	12000	8000	1.02	0.98	62.1	108.9	cal33 ok
04:11:21	NGC 1365	sci36	0.018	12000		1.02	0.98	62.4	111.8	cal33 no photometry
04:18:56	NGC 1365	sci37	0.018	12000		1.02	0.78	62.5	112.9	cal33 no photometry
2008 Apr 22:	**UT3 – UT4**		**081.D-0092(A)**							
06:10:08	HD 107 328	cal41	0.018	8000	4000	1.71	0.66	36.6	118.3	ok
06:52:20	3C 273	sci41	0.018	8000	8000	2.04	0.69	30.7	126.6	cal41 very weak photometry
07:03:47	3C 273	sci42	0.018	8000	8000	2.21	0.59	28.6	129.8	cal41 photometry B contains no signal

[a] From the seeing monitor (DIMM) and at $0.5\,\mu$m.

The second observation of the calibrator HD 083 618 was obtained at the end of the night and no further photometric data could be recorded. The data set was completed using the photometry from the first observation of this calibrator (cal02).

To obtain the final fluxes and the visibility, the two individual measurements of Mrk 1239 were averaged. This is possible because the position angle and baseline length only differ insignificantly.

A.4. NGC 3281

An unsuccessful attempt to observe the Seyfert 2 galaxy NGC 3281 (v_{hel} = 3200 ± 22 km s^{-1}, Theureau et al. 1998; D = 45 Mpc, 1 arcsec = 210 pc) was made during the observing run on 2007 Feb 07. MACAO could not lock on the nucleus of this galaxy because it was too extended in the visible. As a consequence, the source could also not be detected with IRIS and no data were obtained at all.

A.5. NGC 4151

Our first observation of NGC 4151 was carried out on 2007 Feb 07 using the UT2 – UT3 baseline. From the two fringe tracks that were attempted, only the second one contains useful data: the fringes were clearly tracked for about 40 sec before they were lost. Only these 40 sec of tracking were used for the determination of the correlated flux. Due to the failure of MACAO to keep the loop closed on UT2 while chopping, only the photometry for beam A contains useful data. A pipeline reduction with EWS was performed using the A photometry for beam B. The result was double checked by an additional determination of the total flux only using the A photometries of NGC 4151 and of HD 098 430 alone, as described for the first observation of NGC 1365 (see Appendix A.1): the two total flux spectra agree within 30 %.

More successful observations were carried out on 2008 Apr 22 and 2008 Apr 24 with the UT3 – UT4 and the UT2 – UT4 baselines, respectively. These new observations as well as a full analysis for the interferometric data will be presented in a separate paper, Burtscher et al. in preparation.

A.6. 3C 273

3C 273 was first observed during the observation run on 2007 Feb 07. MACAO could not keep the loop closed during chopping and, as a result, no acquisition images and photometry were obtained. Given the pointlike nucleus with V = 12.8 mag (Türler et al. 2006) and the later success closing the loop on the nucleus (see below), the reason for this malfunction remains unexplained. Instead, the beams were aligned with IRIS in the K band alone. In total, four attempts to track fringes were performed, however only the last two contain an interferometric signal. During the data reduction they were treated as a single, long track. Because no photometric data were available, only the calibrated correlated flux could be determined from the MIDI data. To obtain a rough estimate for the total flux of the source, intermediate band photometry with VISIR was obtained on 2007 Mar 01, that is, 23 days after the interferometric observations. VISIR, the VLT Imager and Spectrometer for the mid-InfraRed, provides a long-slit spectrometer as well as a high sensitivity imager in both the N and the Q bands (Lagage et al. 2004). The two filters, in which 3C 273 was observed, were PAH1 (λ_0 = 8.59 μm, $\Delta\lambda$ = 0.42 μm) and SiC (λ_0 = 11.85 μm,

$\Delta\lambda$ = 2.34 μm; Smette & Vanzi 2007). The calibrator star for the VISIR observations was HD 124 294. The VISIR data were reduced by combining the chopped and nodded frames in the standard procedures for such data. The photometry was extracted in a 2.25 arcsec aperture. For the calibration, the template spectrum of HD 124 294 from the catalogue by Roy van Boekel (private comm.) was used. The errors were estimated by increasing the aperture to 3.00 arcsec and by decreasing it to 1.50 arcsec – for both the calibrator and 3C 273 in the opposite way. In the VISIR images most of the flux is contained within 1.5 arcsec and the FWHM of the PSF is 0.39 arcsec and 0.44 arcsec at 8.59 μm and 11.85 μm, respectively. This is only slightly larger than the FWHM of the calibrator star. Therefore, 3C 273 is not resolved by the VISIR imaging.

More successful observations of 3C 273 were obtained on 2008 Apr 22 with the UT3 – UT4 baseline. Two data sets (fringe track plus photometry) were observed directly one after the other in order to increase the signal to noise ratio. They were both reduced together because no significant change in baseline length and orientation took place between the measurements. The photometric measurements have a very low signal to noise ratio. This is mainly due to very strong variations in the background emission that are insufficiently removed by the chopping. In order to get non-negative fluxes for photometry A from the first data set (sci41, see Table A.1), a special removal of the background was carried out by fitting a 5th order polynomial to the sky emission on both sides of the spectrum. During the reduction of the photometry, we noticed that different total flux spectra can be obtained by changing the mask and the position of the sky bands. The alternative results are well represented by the error bars of the photometry from EWS.

A.7. IC 4329A

This target was also observed during the run on 2007 Feb 07. At first, the MACAO units on both telescopes could not keep the loop closed while chopping. During the interferometric measurement, however, a stable AO correction was possible. Strong fringes were found and tracked in two separate fringe tracks (sci27 and sci28, see Table A.1). These were combined and reduced as one data set. Only later after the observation of the corresponding calibrator, HD 123 123 (cal23), a stable AO correction could be achieved also while chopping. The photometry was thus observed in twilight, 1 hour after the fringe tracks. Because no proper alignment of the beams was carried out for the photometry, these are located at different positions on the detector than those of the interferometric signal. By consequence, the masks had to be adjusted accordingly. Still, the fluxes measured in the two beams differ by more than a factor of 2 and must hence be considered with caution.

A.8. NGC 5506

For the galaxy NGC 5506, which contains a Seyfert 1.9 nucleus and is located at a distance of 25 Mpc (v_{hel} = 1850 ± 8 km s^{-1}, Keel 1996; 1 arcsec = 120 pc), observations were attempted on 2007 Feb 07. However, on both telescopes (UT2 and UT3) MACAO could not lock on the extended and faint nucleus. Hence no data were obtained.

A.9. NGC 7469

Two attempts to observe this source were carried out, the first one on 2006 Sep 11 with the baseline UT2 – UT3, the second one on 2007 Nov 24 with the baseline UT3 – UT4.

During the first attempt, a fringe track (sci11, see Table A.1) was successfully performed, although the signal was extremely weak and the position of the OPD was not always determined correctly. As for NGC 1365, there was no AO correction by MACAO for the subsequent observation of the photometry of beam B (UT2). As a result, the single dish spectrum is very extended spatially and it is unclear to what degree it is dominated by background fluctuations. For instance, no pronounced ozone absorption feature at $9.7\,\mu$m is present in the raw data, indicating that most of the signal is actually spurious. We therefore only selected those portions of the photometry for the data reduction where the background residual after chopping is relatively flat. Additionally, the total flux spectrum of the source was only determined by using the information from beam A of the source and that of the associated calibrator HD 220 009 (cal11), as described in Appendix A.1.

During the second attempt to observe NGC 7469, the environmental conditions were similar to those of the first attempt, with moderate wind and the seeing varying between 1.1 arcsec and 1.3 arcsec. This time, however, MACAO obtained a stable AO correction on the nucleus. The source was successfully centered in MIDI after switching from the SiC to the N8.7 filter and increasing the chopping frequency to 2.3 Hz[4]. Very faint fringes could be detected in the fringe search, however these were too faint to assure a stable fringe tracking: in both of the two tracks that were performed, the OPD drifted away from the zero OPD value. From the few frames where an interferometric signal is present, it seems that the correlated flux was on the order of 0.1 to 0.2 Jy, rising towards longer wavelengths. No photometry was observed on this occasion.

References

Antonucci, R. 1993, ARA&A, 31, 473

Arsenault, R., Alonso, J., Bonnet, H., et al. 2003, in Society of Photo-Optical Instrumentation Engineers (SPIE) Conf. Ser., ed. P. L. Wizinowich & D. Bonaccini, Vol. 4839, 174–185

Balestra, I., Bianchi, S., & Matt, G. 2004, A&A, 415, 437

Beckert, T., Driebe, T., Hönig, S. F., & Weigelt, G. 2008, A&A, 486, L17

Beckert, T. & Duschl, W. J. 2004, A&A, 426, 445

Beers, T. C., Kriessler, J. R., Bird, C. M., & Huchra, J. P. 1995, AJ, 109, 874

Beswick, R. J., Pedlar, A., & McDonald, A. R. 2002, MNRAS, 335, 1091

Buchanan, C. L., Gallimore, J. F., O'Dea, C. P., et al. 2006, AJ, 132, 401

Burtscher, L. et al. in preparation, A&A, to be published

Courvoisier, T. J.-L. 1998, A&A Rev., 9, 1

de Vaucouleurs, G., de Vaucouleurs, A., Corwin, Jr., H. G., et al. 1991, Third Reference Catalogue of Bright Galaxies, ed. G. de Vaucouleurs, A. de Vaucouleurs, H. G. Corwin, Jr., R. J. Buta, G. Paturel, & P. Fouque

Díaz-Santos, T., Alonso-Herrero, A., Colina, L., Ryder, S. D., & Knapen, J. H. 2007, ApJ, 661, 149

Elitzur, M. & Shlosman, I. 2006, ApJ, 648, L101

Frogel, J. F., Elias, J. H., & Phillips, M. M. 1982, ApJ, 260, 70

Galliano, E., Alloin, D., Pantin, E., Lagage, P. O., & Marco, O. 2005, A&A, 438, 803

Gitton, P. B., Leveque, S. A., Avila, G., & Phan Duc, T. 2004, in Society of Photo-Optical Instrumentation Engineers (SPIE) Conf. Ser., ed. W. A. Traub, Vol. 5491, 944

Gorjian, V., Werner, M. W., Jarrett, T. H., Cole, D. M., & Ressler, M. E. 2004, ApJ, 605, 156

Gurwell, M. A., Peck, A. B., Hostler, S. R., Darrah, M. R., & Katz, C. A. 2007, in Astronomical Society of the Pacific Conference Series, Vol. 375, From Z-Machines to ALMA: (Sub)Millimeter Spectroscopy of Galaxies, ed. A. J. Baker, J. Glenn, A. I. Harris, J. G. Mangum, & M. S. Yun, 234

Hao, L., Spoon, H. W. W., Sloan, G. C., et al. 2005, ApJ, 625, L75

Hjelm, M. & Lindblad, P. O. 1996, A&A, 305, 727

Hönig, S. F., Beckert, T., Ohnaka, K., & Weigelt, G. 2006, A&A, 452, 459

Hönig, S. F. et al. in preparation a, A&A, to be published

Hönig, S. F. et al. in preparation b, A&A, to be published

Horst, H., Duschl, W. J., Gandhi, P., & Smette, A. 2009, A&A, 495, 137

Houck, J. R., Roellig, T. L., van Cleve, J., et al. 2004, ApJS, 154, 18

Huchra, J., Davis, M., Latham, D., & Tonry, J. 1983, ApJS, 52, 89

Jaffe, W., Meisenheimer, K., Röttgering, H. J. A., et al. 2004, Nature, 429, 47

Jaffe, W. et al. in preparation, A&A, to be published

Jaffe, W. J. 2004, in Society of Photo-Optical Instrumentation Engineers (SPIE) Conf. Ser., ed. W. A. Traub, Vol. 5491, 715

Käufl, H.-U., Sterzik, M. F., Siebenmorgen, R., et al. 2003, in Society of Photo-Optical Instrumentation Engineers (SPIE) Conf. Ser., ed. M. Iye & A. F. M. Moorwood, Vol. 4841, 117–128

Keel, W. C. 1996, ApJS, 106, 27

Kemper, F., Vriend, W. J., & Tielens, A. G. G. M. 2004, ApJ, 609, 826

Kinney, A. L., Schmitt, H. R., Clarke, C. J., et al. 2000, ApJ, 537, 152

Konigl, A. & Kartje, J. F. 1994, ApJ, 434, 446

Krolik, J. H. 2007, ApJ, 661, 52

Krolik, J. H. & Begelman, M. C. 1988, ApJ, 329, 702

Lagage, P. O., Pel, J. W., Authier, M., et al. 2004, The Messenger, 117, 12

Leinert, C., Graser, U., Przygodda, F., et al. 2003, Ap&SS, 286, 73

Lenzen, R., Hartung, M., Brandner, W., et al. 2003, in Society of Photo-Optical Instrumentation Engineers (SPIE) Conf. Ser., ed. M. Iye & A. F. M. Moorwood, Vol. 4841, 944–952

Lindblad, P. O. 1999, A&A Rev., 9, 221

Mattson, B. J. & Weaver, K. A. 2004, ApJ, 601, 771

Meisenheimer, K., Tristram, K. R. W., Jaffe, W., et al. 2007, A&A, 471, 453

Miles, J. W., Houck, J. R., & Hayward, T. L. 1994, ApJ, 425, L37

Minezaki, T., Yoshii, Y., Kobayashi, Y., et al. 2004, ApJ, 600, L35

Nayakshin, S. 2005, MNRAS, 359, 545

Neugebauer, G., Graham, J. R., Soifer, B. T., & Matthews, K. 1990, AJ, 99, 1456

Neugebauer, G. & Matthews, K. 1999, AJ, 118, 35

Pedlar, A., Howley, P., Axon, D. J., & Unger, S. W. 1992, MNRAS, 259, 369

Pier, E. A. & Krolik, J. H. 1992, ApJ, 399, L23

Poncelet, A., Perrin, G., & Sol, H. 2006, A&A, 450, 483

Prieto, M. A., Reunanen, J., Tristram, K. R. W., et al. in preparation, ApJ, to be published

Raban, D., Heijligers, B., Röttgering, H., et al. 2008, A&A, 484, 341

Raban, D., Jaffe, W., Röttgering, H., Meisenheimer, K., & Tristram, K. R. W. 2009, MNRAS, 394, 1325

Radomski, J. T., Piña, R. K., Packham, C., et al. 2003, ApJ, 587, 117

Risaliti, G., Salvati, M., Elvis, M., et al. 2009, MNRAS, 393, L1

Roche, P. F., Aitken, D. K., Smith, C. H., & Ward, M. J. 1991, MNRAS, 248, 606

Rodríguez-Ardila, A. & Mazzalay, X. 2006, MNRAS, 367, L57

Rousset, G., Lacombe, F., Puget, P., et al. 2003, in Society of Photo-Optical Instrumentation Engineers (SPIE) Conf. Ser., ed. P. L. Wizinowich & D. Bonaccini, Vol. 4839, 140–149

Schartmann, M., Meisenheimer, K., Camenzind, M., et al. 2008, A&A, 482, 67

Schartmann, M., Meisenheimer, K., Klahr, H., et al. 2009, MNRAS, 393, 759

Schmidt, M. 1963, Nature, 197, 1040

Siebenmorgen, R., Krügel, E., & Spoon, H. W. W. 2004, A&A, 414, 123

Silbermann, N. A., Harding, P., Ferrarese, L., et al. 1999, ApJ, 515, 1

Smette, A. & Vanzi, L. 2007, VISIR User Manual, Tech. rep., VLT-MAN-ESO-14300-3514, Issue 80

Soifer, B. T., Bock, J. J., Marsh, K., et al. 2003, AJ, 126, 143

Swain, M., Vasisht, G., Akeson, R., et al. 2003, ApJ, 596, L163

Theureau, G., Bottinelli, L., Coudreau-Durand, N., et al. 1998, A&AS, 130, 333

Tristram, K. R. W. 2007, PhD thesis, Max-Planck-Institut für Astronomie, Königstuhl 17, 69117 Heidelberg, Germany

Tristram, K. R. W., Meisenheimer, K., Jaffe, W., et al. 2007, A&A, 474, 837

Türler, M., Chernyakova, M., Courvoisier, T. J.-L., et al. 2006, A&A, 451, L1

Wada, K. & Norman, C. A. 2002, ApJ, 566, L21

Weedman, D. W., Hao, L., Higdon, S. J. U., et al. 2005, ApJ, 633, 706

Wegner, G., Bernardi, M., Willmer, C. N. A., et al. 2003, AJ, 126, 2268

Wilson, A. S. & Tsvetanov, Z. I. 1994, AJ, 107, 1227

Wittkowski, M., Kervella, P., Arsenault, R., et al. 2004, A&A, 418, L39

---

[4] The chopping frequency was set to a non-integer number in order to not have the same frequency as the gas-helium closed-cycle cooler of MIDI which runs at 1 Hz. This should cancel out any differences in the background between target and sky position, which may be caused by a slight temperature change or vibrations with the frequency of the cooler.